

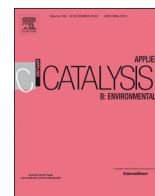


ELSEVIER

Contents lists available at ScienceDirect

## Applied Catalysis B: Environmental

journal homepage: [www.elsevier.com/locate/apcatb](http://www.elsevier.com/locate/apcatb)



# One-pot hydrogen production and cascade reaction of furfural to bioproducts over bimetallic Pd-Ni TUD-1 type mesoporous catalysts

Margarida M. Antunes<sup>a</sup>, Sérgio Lima<sup>b</sup>, Auguste Fernandes<sup>c</sup>, Maria F. Ribeiro<sup>c</sup>, David Chadwick<sup>b</sup>, Klaus Hellgardt<sup>b</sup>, Martyn Pillinger<sup>a</sup>, Anabela A. Valente<sup>a,\*</sup>

<sup>a</sup> Department of Chemistry, CICECO-Aveiro Institute of Materials, University of Aveiro, Campus Universitário de Santiago, 3810-193, Aveiro, Portugal

<sup>b</sup> Department of Chemical Engineering, Imperial College London, South Kensington Campus, London, SW7 2AZ, UK

<sup>c</sup> Centro de Química Estrutural (CQE), Instituto Superior Técnico, Universidade de Lisboa, Av. Rovisco Pais, 1049-001, Lisbon, Portugal

## ARTICLE INFO

### Keywords:

Furfural  
Bioproducts  
Bimetallic catalysts  
Mesoporous TUD-1  
Hydrogen carrier

## ABSTRACT

Bimetallic Pd-Ni TUD-1 type mesoporous catalysts are effective for the cascade reaction of the renewable platform chemical furfural (FUR) to the useful bioproducts 2-alkoxyfuran, 2-methylfuran (2MF), 4-oxopentanal and its acetals, which find diverse applications, some already in the market. With a single catalyst, the in situ hydrogen supply from formic acid (FAC), as well as several acid-reduction steps of the overall catalytic process were triggered, leading to the desired bioproducts (bioPs), all in one-pot under moderate reaction conditions. These multipurpose materials were prepared using different procedures and conditions, which influenced the material properties and the catalytic performances. Detailed characterisation (microstructural/molecular level) and catalytic studies led to new mechanistic insights into the FUR reaction (with identification of intermediates), allowed to assess the roles of the different types of metal species in the complex reaction mechanism, understand the influence of material properties on the catalytic process, and catalyst stability and regeneration. The best-performing catalyst was prepared stepwise via impregnation of palladium on a hydrothermally synthesised nickel silicate with a molar ratio Si/Ni of 20, ending with filtration-washing-calcination procedures. This catalyst led to 83% 2MF yield, at 98% FUR conversion (90% total bioPs yield), using 1-butanol as solvent, at 170 °C. The reported catalytic protocol benefits from the fact that external usage of H<sub>2</sub> for catalyst activation and/or the catalytic reaction is not required, no high-pressure gases are used, and FAC is used as source of hydrogen supplied in situ for the catalytic reaction under moderate conditions. Moreover, FAC presents low toxicity, it is easy to handle/store, and is a typical coproduct of carbohydrate biomass conversion processes, and thus its re-purposing is highly desirable.

## 1. Introduction

Furfural (FUR) is a renewable platform chemical used for manufacturing various bio-based consumer products [1–8]. It is produced from vegetable waste matter (e.g. sugar cane bagasse, corncobs, oat/rice hulls), and its valorisation is highly desirable for the global bio-based economy. Most relevant synthesis and conversion routes of FUR involve acid and reduction chemistry [6,8–18]. One of the most important steps of FUR conversion is its reduction to furfuryl alcohol (FA), which is the highest production volume chemical from FUR (ca. 65%) [9,10,13]. The wide applications profile of FA partly results from its high reactivity and low viscosity, being used in different industrial sectors such as refractory, foundry, polymer, drugs, fragrances, etc. [3,9,10,19–24]. The reduction of FUR may lead to a wide spectrum of useful bioproducts, as highlighted in several very interesting reviews

for many different types of catalysts and catalytic reaction conditions (batch or continuous-flow; atmospheric to high pressure; ambient to high temperature; and with or without requirement for a stage of catalyst pre-reduction with externally supplied H<sub>2</sub> at high temperature) [7,9,10,16,23,25,26].

Recent and emerging applications of FUR/FA include their use as intermediates for synthesising useful 2-alkoxyfuran (AoFs), 2-methylfuran (2MF), and pentanediol/dione products, with diverse applications (Scheme 1). For example, AoFs are interesting flavours, some already commercialised [27,28], and markers for beer storage conditions [27]. 2MF is a useful bio-based solvent [9,10], and intermediate for producing pesticides [9,29–34], perfumes and drugs [29–34]. Both AoF and 2MF may combine good fuel performance with moderate FUR upgrade footprint (in terms of investment costs, CO<sub>2</sub> emission), as reported by Lange et al. [7] based on fuel evaluation studies. AoFs are recognised as

\* Corresponding author.

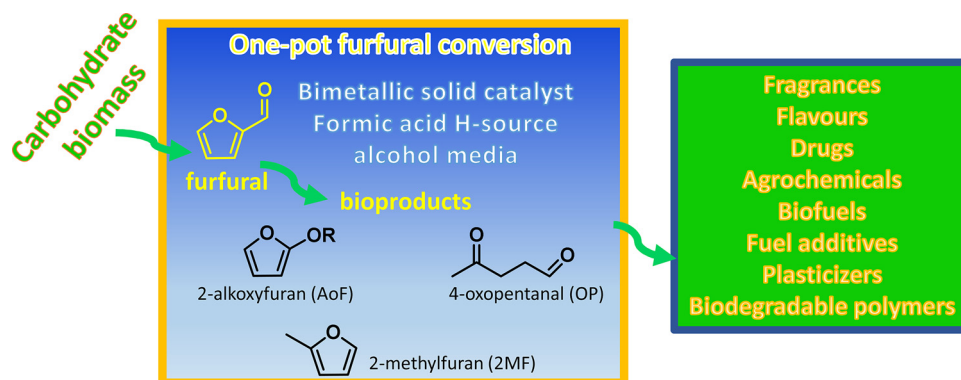
E-mail address: [atav@ua.pt](mailto:atav@ua.pt) (A.A. Valente).

<https://doi.org/10.1016/j.apcatb.2018.06.004>

Received 23 March 2018; Received in revised form 31 May 2018; Accepted 2 June 2018

Available online 04 June 2018

0926-3373/ © 2018 Elsevier B.V. All rights reserved.



**Scheme 1.** Carbohydrate biomass-derived furfural (FUR) may be converted to the useful bioproducts 2-(alkoxymethyl)furan, 2-methylfuran, 4-oxopentanal and its acetals, via acid-reduction chemistry, using a hydrogen source, and a bimetallic heterogeneous catalyst, in alcohol media.

interesting fuel blend components [7,35–39], and 2MF as an attractive fuel or fuel additive [7,8,10,13,14,23,30,34]. 2MF possesses properties comparable to conventional gasoline [25,30] and promising production efficiency [14]. A road trip study of a mixture of 2MF plus gasoline indicated 2MF as an economically promising biofuel, with no negative impact on regulated vehicle emissions [7]. It was reported higher thermal efficiency for 2MF than gasoline (based on engine tests) [40], and emissions were lower for 2MF [9,41]. 2MF may be converted to high quality synthetic diesel range products [9,41]. Since 2MF is somewhat hydrophobic, it may be easily separated from water at room temperature [41,42]. In particular, the reaction of 2MF with 4-oxopentanal (OP) gives diesel range alkanes where water is the sole coproduct, presenting a promising clean route [6,9,41–43]. Other biomass conversion routes involve OP as intermediate to 1,4-pentanediol [9,44,45], which may be upgraded to plasticisers [9,23], biodegradable polyesters [13,22,46], and biofuels [16]; acetals of OP, such as 5,5-diethoxy-2-pentanone are useful for synthesising terpenic flavourings [47,48].

The conversion of FUR to the bioproducts (bioPs) AoFs, 2MF and OP involves cascade acid and reduction reactions (Scheme 1). The reduction pathways call for the use of a reducing agent, which is conventionally high-pressure  $H_2$ , or alternatively an organic H-carrier. The in situ hydrogen supply for reduction reactions may enhance the reactant-catalyst surface interactions, and thus the overall kinetics [49]. In particular, formic acid (FAC) is an attractive H-source [50–52], and its use presents several advantages over the external usage of high-pressure  $H_2$ , such as safe transport and storage, and relatively low toxicity [49,50,53,54]. FAC is cheap, and a typical coproduct of carbohydrate biomass conversion processes, and thus its repurposing is highly desirable [12,50,53–57]. The FUR conversion to bioPs requires the use of appropriate catalysts, preferably a single efficient multifunctional heterogeneous catalyst that enables the in situ hydrogen supply from FAC, as well as the cascade FUR conversion.

In an outstanding review by Lange [58] regarding the problem of catalyst deactivation for biomass conversion processes in liquid polar media, it was emphasized that catalytic hydrogenation routes may require the use of noble metal catalysts for overcoming leaching phenomena which is expected for non-noble metal catalysts. The relevant role of noble metal catalysts in biomass conversion to fuels and chemicals was recently reviewed by Makhubela and Darkwa [59], highlighting several commercial/pilot-scale projects by companies such as Johnson Matthey (UK), GFBiochemicals (Italy), Avantium (The Netherlands), BASF (Germany), Anellotech (USA), Quaker Oats (USA), Rennovia (USA), and Changchun Dacheng Group (China). Noble metal catalysts may effectively convert FAC to  $H_2$  [49,50,52,54,60–63]. In particular, Mori et al. [61] highlighted the effectiveness of palladium-based nanoparticles for selectively converting FAC to  $H_2$ . Various biomass conversion processes involving reduction chemistry have been

successfully carried out using FAC and palladium-based heterogeneous catalysts. Examples include: crude biomass such as Jatropha oil to hydrocarbons over Pd/C [60], and peanut, corn, soybean oils, soybean lecithin to fatty acids over Pd/C catalysts [64]; fructose and 5-hydroxymethylfurfural (HMF) to 2,5-dimethylfuran (DMF) over Pd/C (plus  $H_2SO_4$ ) [65,66]; HMF to 1,6-hexanediol over Pd supported on ZrP, HY,  $Nb_2O_5$ , ZSM-5,  $SiO_2-Al_2O_3$ ,  $Al_2O_3$  or  $SO_4/ZrO_2$  [67]; hydrogenation of sugar derivatives over Pd/C [68], levulinic acid (LA) to  $\gamma$ -valerolactone (GVL) [69] over alumina-supported Pd [70], condensation of FUR and cyclopentanone and further hydrogenation over Pd/C [71]; lignin to simple aromatics/phenolic monomers over Pd-NafionSAC-13 [72], Pd/ $Al_2O_3$  [73] or Al-SBA-15-supported Pd nanoparticles [74]; bio-oil hydroprocessing over zeolite-supported Pd [49]; upgrading vanillin over N-enriched mesoporous carbon-supported Pd [75]; and bimetallic Pd-Ag alloy supported on  $Fe_3O_4/N_2$  doped reduced graphene oxide [76]. It is known from the literature that synergetic effects of catalyst composition and cost effectiveness may be obtained by using bimetallic supported catalysts for FAC conversion to  $H_2$  [61,76,77].

In this work, the one-pot conversion of FUR to the bioproducts AoFs, 2MF, OP and its acetals, was investigated using FAC as the source for in situ hydrogen supply, and bimetallic Pd-Ni TUD-1 type mesoporous catalysts, where palladium and nickel species played roles in the reduction and acid chemistry, respectively, of the cascade reaction system. The TUD-1 type materials were chosen partly because they may be prepared via eco-friendly non-surfactant templating routes [78–80]. The nickel species were introduced in the materials during the hydrothermal synthesis of the TUD-1 type matrix, aiming at uniform metal distribution and enhanced metal-support interactions; then palladium was impregnated on the nickel silicates via different procedures/conditions, strategically leading to multipurpose bimetallic materials. The catalytic protocol advantageously does not require external usage of  $H_2$  for catalyst pre-treatment or the catalytic reaction, nor any high-pressure gas, by using a multipurpose material that not only enables the formation of the bioproducts, but is also capable of generating hydrogen in situ from FAC, which is a typical coproduct of carbohydrate biomass conversion processes, and thus its repurposing is highly desirable.

## 2. Experimental

### 2.1. Materials

Triethanolamine (TEA, 98%, Sigma-Aldrich), tetraethylammonium hydroxide (TEAOH, 35 wt.% in  $H_2O$ , Aldrich), Palladium(II) nitrate dihydrate ( $Pd(NO_3)_2 \cdot 2H_2O$ , ca. 40% Pd basis, Aldrich), tetraethylorthosilicate (TEOS, 98%, Sigma-Aldrich), nickel(II) nitrate hexahydrate ( $Ni(NO_3)_2 \cdot 6H_2O$ , 98.5%, Sigma-Aldrich), deionised water (DI water), furfural (FUR, 99%, Aldrich), furfuryl alcohol (FA, 99%,

Aldrich), 2-ethoxyfuran (EoF, 97%, Manchester Organics), ethyl levulinate (EL, 99%; Aldrich), 2-methylfuran (2MF, analytical standard; Sigma-Aldrich), 4-oxopentanol (OP, 95%; Toronto Research Chemicals),  $\alpha$ -angelica lactone (AnL, 98%, Alfa Aesar), absolute ethanol (EtOH, analytical grade, ACS Reag. pH Eur, 99.9%, Scharlau), 1-butanol (BuOH, ACS  $\pm$  99.4%, Alfa Aesar), formic acid (FAc, 98%, Fluka), ammonium formate (PA, 97%; Aldrich), acetic acid (100%, Merck).

## 2.2. Synthesis of the materials

The nickel silicates of the type TUD-1 (NiTUD(x)) were prepared with different molar ratios Si/Ni (Si/Ni =  $x$  = 10, 20, 50) in a similar fashion to that described in the literature [81]. TEOS and nickel(II) nitrate hexahydrate were the Si and Ni sources, respectively. For example, for  $x$  = 10, a mixture of nickel(II) nitrate hexahydrate (4.63 g) and water (3.12 g) was added to TEOS (33.2 g), and stirred for 5 min. Afterwards, a mixture of TEA (24.7 g) and water (6.76 g) was added with vigorous stirring for 2 h until a gel was obtained. Then, TEOH aqueous solution (33.2 g) was added with vigorous stirring. The obtained synthesis gel was aged under static conditions, at room temperature for 24 h, and then dried at 98 °C for 24 h. The obtained solids were gently grinded using an agate mortar and pestle, and then transferred into a Teflon-lined autoclave, followed by hydrothermal treatment at 180 °C for 8 h. Finally, the solids were calcined at 600 °C for 10 h in static air (heating rate of 1 °C min<sup>-1</sup>), giving NiTUD(x). The materials were grinded using an agate mortar and pestle, and subsequently sieved to give a powder with particle sizes in the range 90–250  $\mu$ m.

The yPdNiTUD(x) materials (palladium load of 1.5 wt% ( $y$  = 1) or 7 wt% ( $y$  = 7)) were prepared via the incipient wetness impregnation method, with solvent evaporation (IWI). For example, for  $y$  = 7, an aqueous solution of palladium(II) nitrate dihydrate (ca. 40% Pd, 0.3761 g, 1.41 mmol) in deionised water (4 mL) was added to NiTUD(x) (2 g), and stirred for 2 h, at room temperature. The solvent was evaporated at 110 °C overnight, and the dried solids were calcined at 500 °C (heating rate of 2 °C min<sup>-1</sup>) for 6 h, giving the materials 7PdNiTUD(x). In a different procedure (denoted FW), the aqueous suspensions of NiTUD(x) and the palladium precursor were stirred for 2 h, at room temperature, filtered (F), washed (W) with deionised water at room temperature, followed by drying at 110 °C overnight, and finally calcined under similar conditions as those used for yPdNiTUD(x), giving the materials yPdNiTUD(20)w.

For comparative studies, mesoporous silica TUD-1 and aluminosilicate Al-TUD-1 were used as supports for palladium (7 wt.%) via the IWI procedure. TUD-1 was prepared following a similar procedure to that for NiTUD(x), but without adding nickel(II) nitrate to the synthesis gel. Al-TUD-1 was prepared as described previously [82,83]; aluminium isopropoxide (1.66 g) was added to a mixture of ethanol (8 mL), anhydrous 2-propanol (13 mL) and TEOS (25.0 g, 0.12 mol), under stirring at 45 °C (synthesis gel with a molar ratio Si/Al of 20). Then, a mixture of TEA (25 g, 0.17 mol) and DI water (18.8 g, 1.04 mol) was added. The total mixture was stirred for 2 h, followed by addition of TEOH (22.4 g) under vigorous stirring. The resultant gel was subsequently aged for 24 h (under static conditions), and dried at 98 °C, for 24 h. The obtained solid was gently grinded, followed by hydrothermal treatment in a Teflon-lined autoclave for 8 h, at 180 °C. Finally, the material was calcined at 600 °C (static air) for 10 h (heating rate of 1 °C min<sup>-1</sup>) in order to remove the organic template and synthesis by-products.

## 2.3. Characterisation of the materials

Powder X-ray diffraction (PXRD) data were collected on an Empyrean PAN analytical diffractometer (Cu-K $\alpha$  X radiation,  $\lambda$  = 1.54080 Å) in a Bragg-Brentano para-focusing optics configuration (45 kV, 40 mA). Bulk PdO and NiO were prepared in spinning flat-plate

sample holders and step-scanned in the range 3–68 ° (2 $\theta$ ) with a step size of 0.026°. A PIXEL linear detector with an active area of 1.7462° was using with a counting time of 70 s per step. The remaining samples (deposited between acetate foils) were analysed in a single setup using (CuK $\alpha$  X-radiation) with Ni filter, a linear PIXEL1D detector with an active length of 3.74°, a fixed divergence slit of 1/8°, and a spinner sample holder, in transmission mode using a focusing optics mirror configuration. Intensity data were collected by the continuous counting method (step size of 0.013° in the range 10–70° 2 $\theta$ , with a counting time of 800 s per step) during  $\approx$  4 h.

The average crystallite size determination was based on the profile analysis refinement using Highscore Plus (Panalytical) in the range 30–70° 2 $\theta$  for the following parameters for Ni and Pd phases: structural; one overall isotropic temperature factor; one scale factor, three half-width (a Pseudo-Voigt peak shape function was used), cell parameters, and no asymmetry parameters; global, one displacement point, and three coefficients of polynomial background. The structure values used for refinement were extracted from references ICDD 04-004-5421 for palladium oxide and 04-013-0886 for nickel oxide. The crystallite size was calculated from the Lorentzian component of experimental peaks after Instrumental Resolution Function subtraction.

For the TUD-1 type materials, low-angle (0.5–5° 2 $\theta$ ) PXRD was carried out using the transmission mode; the sample was deposited between Mylar foils, and step-scanned in 0.013° (2  $\theta$ ) steps with a counting time of 80 s per linear detector active area of 2.0°.

The images of morphology and high resolution elemental mappings (Si, Ni, Pd) were obtained by scanning transmission electron microscopy (STEM) using a Hitachi HD2700 scanning transmission electron microscope, equipped with a Bruker EDS detector. Samples were prepared by depositing a drop of the solid sample in ethanol onto holey amorphous carbon-film-coated 400 mesh copper grids (Agar Scientific).

Inductively coupled plasma atomic emission spectroscopy (ICP-AES) analyses were performed at the Central Analysis Laboratory (University of Aveiro). The measurements were carried out using a Horiba Jobin Yvon Activa W spectrometer (detection limit of ca. 20  $\mu$ g L<sup>-1</sup>; experimental range of error of ca. 5%). Prior to analyses, the solids (15 mg) were digested using 1 mL of HF and 0.5 mL of HNO<sub>3</sub> and microwave heated at 180 °C (heating rate of 5 °C min<sup>-1</sup>) during 5 min, for quantification of Si and Ni; for the quantification of Pd, the digestion was performed using 3 mL of HCl and 1 mL of HNO<sub>3</sub>.

Nitrogen adsorption-desorption isotherms were obtained at -196 °C using a Micromeritics GeminiV 2380. The samples were pre-treated at 300 °C for 3 h. The calculated textural parameters were as follows: the specific surface area ( $S_{\text{BET}}$ ) using the BET equation, the total pore volume at a relative pressure ( $p/p_0$ ) of ca. 0.98 using the Gurvitsch rule. The mesopore size distribution curves were calculated from the adsorption data using the BJH method.

The reduction properties of the materials were investigated by temperature-programmed reduction with hydrogen (TPR-H<sub>2</sub>), using a Micromeritics Autochem II Chemisorption Analyzer. The samples were pre-treated in air at 300 °C (heating rate of 10 °C min<sup>-1</sup>) for 30 min. The gas flow was changed from air to argon and the sample was cooled to 30 °C, and left at that temperature for 30 min. The gas flow was then changed to 5% H<sub>2</sub>:argon, during 30 min, at 30 °C, prior to analysis. The samples were heated until 950 °C (heating rate of 10 °C min<sup>-1</sup>); water was trapped using solid CO<sub>2</sub>. The H<sub>2</sub> consumption was calculated via deconvolution of the TPR-H<sub>2</sub> curves, and integration of the peaks, based on pre-calibrations.

The acid properties were measured by Fourier-transform infrared spectroscopy (FT-IR) of adsorbed pyridine, using a Nexus Thermo Nicolet apparatus (64 scans and resolution of 4 cm<sup>-1</sup>) equipped with a homemade vacuum cell, and using self-supported discs (5–10 mg cm<sup>-1</sup>) and pyridine as the base probe. After in situ outgassing at 350 °C for 3 h (10<sup>-6</sup> mbar), pyridine (99.99%) was contacted with the sample at 150 °C for 10 min, and subsequently evacuated at 150 °C and 250 °C for 30 min under vacuum (10<sup>-6</sup> mbar). The IR band at ca. 1455 cm<sup>-1</sup> due to

pyridine adsorbed on Lewis (L) acid sites was used for quantification [84]. For evaluating the L acid strength, the molar ratio of moderately strong to total acid sites is taken as the ratio  $L_{250}/L_{150}$ , where  $L_T$  ( $T = 150$  or  $250^\circ\text{C}$ ) is the amount of L acid sites that remained in the solid material after desorption at temperature  $T$ .

## 2.4. Catalytic tests

The catalytic experiments were performed in tubular glass pear-shaped reactors, equipped with an appropriate polytetrafluoroethylene (PTFE)-coated magnetic stirring bar and a valve. In a typical procedure, FUR (0.26 M), powdered catalyst (loading of  $12.8\text{ g}_{\text{cat}}\text{ L}_{\text{mix}}^{-1}$ ), formic acid (FAC) as reducing agent (0.28 mL), and 1 mL of the alcohol (ROH; ethanol (EtOH) or 1-butanol (BuOH)) were added to the reactor. Sometimes, reaction intermediates were used instead of FUR. Ammonium formate and acetic acid were also tested as reducing agents. The reactor was immersed in a thermostatically controlled oil bath heated at  $140$  or  $170^\circ\text{C}$  with a stirring rate of  $1000\text{ rpm}$ , which was taken as the instant that the reaction began (zero time).

Catalyst stability studies involved reuse of the recovered catalyst, a contact test (CT), and characterisation of the used catalysts.

The CT was carried out to study the solvothermal stability of the catalyst, and specifically to check for the catalytic contribution of dissolved active metal species. Firstly, the original catalyst was contacted with EtOH/FAC, at  $140^\circ\text{C}$ , for 24 h, under similar conditions to those used for the normal catalytic tests, but without substrate. Subsequently, the mixture was cooled to ambient temperature, and passed through a filter containing a  $0.2\text{ }\mu\text{m}$  PTFE membrane. The liquid obtained from the CT (EtOH/FAC) was transferred to a separated clean reactor, and FUR was added to give an initial concentration of  $0.26\text{ M}$  (similar to that for a normal catalytic test). The homogeneous reaction mixture (FUR/EtOH/FAC) was then heated at  $140^\circ\text{C}$ , for 24 h, with stirring ( $1000\text{ rpm}$ ). The catalytic results were compared to those for a normal catalytic test (without catalyst filtration). On the other hand, the catalysts (7PdNiTUD(10), 7PdNiTUD(20 w)) were used for three consecutive (normal) catalytic batch runs, under similar reaction conditions (FUR/FAC/EtOH, 24 h,  $140^\circ\text{C}$ ). Catalyst recovery involved separation of the solid from the reaction mixture by centrifugation, through washing with EtOH, drying overnight at  $85^\circ\text{C}$  in atmospheric air, and treatment at  $500^\circ\text{C}$  in static air for 4 h (heating rate of  $1^\circ\text{C min}^{-1}$ ).

## 2.5. Quantification and identification of products

The evolution of the catalytic reactions was monitored by GC for quantification of the products, and HPLC for quantification of FUR. The reactors were cooled to ambient temperature in cold water before opening, and suitable work-up procedures. The analyses were always carried out for freshly prepared samples. The GC analyses were carried out by using a Varian 3800 instrument equipped with a capillary column (VF-5 ms,  $30\text{ m} \times 0.25\text{ mm} \times 0.25\text{ }\mu\text{m}$ ) and a flame ionisation, with  $\text{H}_2$  as the carrier gas. The HPLC analyses were carried out by using a Knauer Smartline HPLC Pump 100 and a Shodex SH101H<sup>+</sup>  $300 \times 8\text{ mm}$  (internal diameter) ion exchange column (Showa Denko America, Inc., New York), coupled to a Knauer Smartline UV detector 2520 ( $254\text{ nm}$ ). The mobile phase was  $0.005\text{ M aq H}_2\text{SO}_4$  at a flow rate of  $0.8\text{ mL min}^{-1}$ , and the column temperature was  $50^\circ\text{C}$ . Calibration curves were measured for quantification by GC and HPLC. Individual experiments were performed for a given reaction time, and the presented results are the mean values of at least two replicates (experimental error in the range 3–5 %).

The substrate (sub) conversion (%) at a reaction time  $t$  was calculated by using the formula  $100 \times [(\text{initial molar concentration of sub}) - (\text{molar concentration of sub at time } t)]/(\text{initial concentration of sub})$ . The yield (%) of product (pro) at reaction time  $t$  was calculated by using the formula  $100 \times [(\text{molar concentration of pro at time } t)]/(\text{initial$

molar concentration of sub)]. In the reaction of FUR, the bioproducts formed were 2-alkoxyfurans (EoF and BoF for alkoxy = ethoxy or butoxy, respectively), 2-methylfuran (2MF), 4-oxopentanal (OP), and acetals of OP (OPea where ea is ethyl acetal, formed when using EtOH; OPba where ba is butyl acetal, formed when using BuOH). OPea or OPba stands for the sum of the isomers 5,5-dialkoxy-2-pentanone and 2,2-dialkoxy-5-pentanal.

The products were identified using a Trace GC 2000 Series (Thermo Quest CEInstruments)-DSQ II (Thermo Scientific) instrument, equipped with a DB-1 capillary column ( $25\text{ m} \times 0.25\text{ nm}$ ;  $0.25\text{ }\mu\text{m}$ ), with He as the carrier gas, and using the commercial databases Wiley 6 and NIST Mainlib and Replib. The MS data for the bioPs are as follows. 2-Ethoxyfuran (EoF),  $m/z$  (relative intensity): 126 [ $\text{M}^+$ ] (20), 98 (7), 97(16), 95(3), 83 (2), 82 (32), 81(100), 70 (20), 69 (38), 54 (13), 53 (14), 41 (60), 28 (7). 2-Butoxyfuran (BoF),  $m/z$  (relative intensity): 155 [ $\text{M}^+ + 1$ ] (2), 154 [ $\text{M}^+$ ] (21), 98 (6), 97 (9), 95 (2), 83 (2), 82 (26), 81 (100), 70 (4), 57 (3), 53 (9), 41 (6), 39 (7), 32 (7), 28 (29). 4-Oxopentanal (OP),  $m/z$  (relative intensity): 100 [ $\text{M}^+$ ] (0.2), 85 (7), 73 (3), 72 (65), 58 (6), 57 (13), 55 (2), 44 (0), 43 (100), 32 (22), 31 (11). 2-Methylfuran (2MF),  $m/z$  (relative intensity): 84 [ $\text{M}^+ + 2$ ] (2), 83 [ $\text{M}^+ + 1$ ] (30), 82 [ $\text{M}^+$ ] (100), 81 (58), 55 (12), 54 (22), 53 (33), 52 (5), 51 (6), 50 (6), 46 (5), 45 (13), 43 (3), 39 (8), 38 (2). 5,5-Diethoxy-2-pentanone,  $m/z$  (relative intensity): 173 [ $\text{M}^+ - 1$ ] (0.6), 130 (7), 129 (94), 128 (0), 117 (1), 116 (18), 104 (6), 103 (100), 101 (32), 99 (9), 85 (12), 84 (6), 83 (60), 75 (49), 71(4), 59 (9), 58 (3), 57 (11), 55 (20), 47 (34), 43 (28), 41 (4), 29 (4). 5,5-Dibutoxy-2-pentanone,  $m/z$  (relative intensity): 229 [ $\text{M}^+ + 1$ ] (1), 173 (1), 160 (4), 159 (37), 158 (11), 157 (100), 143(0.4), 117 (6), 103 (15), 102 (4), 101 (56), 100 (6), 99 (10), 84 (3), 83 (25), 71 (3), 61 (6), 57 (44), 55 (7), 43 (12), 41 (14), 29 (7), 28 (2), 18 (2). 2,2-Diethoxy-5-pentanal,  $m/z$  (relative intensity): 173 [ $\text{M}^+ + 1$ ] (3), 160 (1), 159 (10), 131 (1), 130 (7), 129 (100), 128 (7), 103 (3), 101 (19), 100 (10), 99 (11), 86 (6), 85 (15), 83 (21), 72 (14), 71 (5), 59 (3), 58 (12), 57 (13), 55 (9), 45 (2), 43 (13). 2,2-Dibutoxy-5-pentanal,  $m/z$  (relative intensity): 229 [ $\text{M}^+ - 1$ ] (0.6), 215 (4), 207 (0.3), 180 (0.3), 159 (3), 158 (11), 157 (100), 128 (1), 115 (2), 103 (3), 102 (2), 101 (37), 100 (2), 99 (6), 85 (5), 84 (4), 83 (12), 73 (4), 72 (6), 71 (1), 59 (2), 58 (6), 57 (8), 55 (4), 43 (8), 41 (7), 39 (2), 29 (2), 28 (1), 27 (0.5), 18 (0.5).

## 3. Results and discussion

### 3.1. Characterisation of the materials

The nickel silicates NiTUD(x) were hydrothermally synthesised using molar ratios Si/Ni (x) of the synthesis gel of 10, 20 and 50, and the obtained materials possessed bulk Si/Ni ratios (measured by ICP-AES) of 8, 16 and 47, respectively (Table 1), which are comparable to those of the synthesis gels. NiTUD(x) were used to support palladium (1.5 wt% ( $y = 1$ ), or 7 wt% ( $y = 7$ )) via incipient wetness impregnation-solvent evaporation-calcination (IWI method), or impregnation-filtration-washing-calcination (FW procedure). The materials possessed bulk molar ratios Si/(Ni + Pd) in the range 9–34, being higher for 1PdNiTUD(x) than the related 7PdNiTUD(x) material, which is consistent with higher amount of palladium used for preparing the latter. The FW procedure ( $x = 20$ ) led to slightly higher Si/(Ni + Pd) ratio than the IWI method, suggesting the partial removal of (weakly adsorbed) metal species in the washing step of the FW procedure.

The low-angle PXRD patterns of all TUD-1 type materials prepared showed a broad peak centred at ca.  $1.5^\circ 2\theta$  (Fig. S1), suggesting that the materials possessed a somewhat defined mesopore size distribution, which is consistent with the  $\text{N}_2$  adsorption results, discussed ahead. Fig. 1 shows the wide-angle PXRD patterns of the mono- and bimetallic materials, and, for comparison, commercial bulk NiO and PdO. Commercial NiO exhibited very narrow peaks (high crystallinity) at  $2\theta \cong 37^\circ, 44^\circ, 63^\circ$  assignable to a hexagonal crystal system with R3m space group (ICDD No. 04-013-0886). Commercial PdO exhibited very

**Table 1**  
Composition and textural properties of the mono- and bimetallic TUD-1 type materials.

Sample	Composition <sup>a</sup>		Textural properties <sup>b</sup>		
	Si/Ni	Si/(Ni + Pd)	$S_{\text{BET}}$ ( $\text{m}^2\text{g}^{-1}$ )	$V_p$ ( $\text{cm}^3\text{g}^{-1}$ )	$D_p^c$ (nm)
NiTUD(10)	8	–	456	0.8	12
1PdNiTUD(10)	12	11	409	0.7	11
7PdNiTUD(10)	12	9	399	0.7	12
NiTUD(20)	16	–	350	1.0	24–32
1PdNiTUD(20)	18	15	292	1.0	32
1PdNiTUD(20)w	21	17	300	1.0	32
7PdNiTUD(20)	22	10	297	1.0	24–32
7PdNiTUD(20)w	25	13	321	0.9	19–31
NiTUD(50)	47	–	405	0.9	19
1PdNiTUD(50)	47	34	387	0.9	15
7PdNiTUD(50)	57	18	353	0.9	15
7PdAlTUD-1	23 <sup>d</sup>	–	586	0.8	7
7PdTUD-1	–	–	419	0.8	16
TUD-1	–	–	532	0.9	16

<sup>a</sup> Molar ratios determined by ICP-AES.

<sup>b</sup> Based on  $\text{N}_2$  sorption isotherms at  $-196^\circ\text{C}$ .

<sup>c</sup> Pore size distributions determined by the BJH method using the  $\text{N}_2$  adsorption data.

<sup>d</sup> The value corresponds to the molar ratio Si/Al.

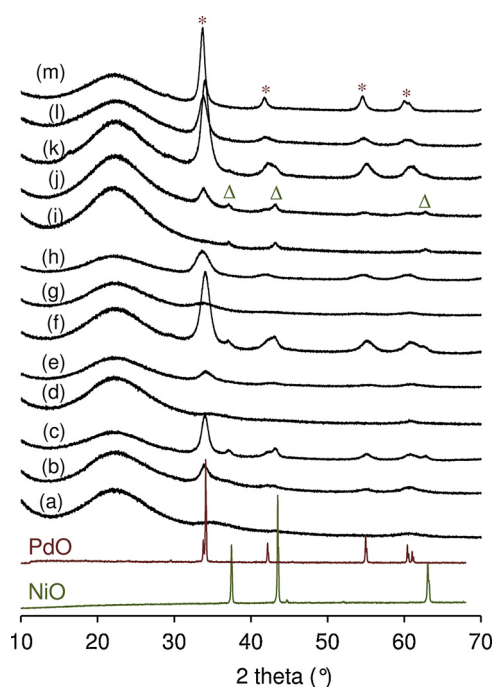


**Fig. 1.** Wide-angle PXRD patterns of NiTUD(10) (a), 1PdNiTUD(10) (b), 7PdNiTUD(10) (c), NiTUD(20) (d), 1PdNiTUD(20) (e), 7PdNiTUD(20) (f), 1PdNiTUD(20)w (g), 7PdNiTUD(20)w (h), NiTUD(50) (i), 1PdNiTUD(50) (j), 7PdNiTUD(50) (k), 7PdAlTUD-1 (l), 7PdTUD-1 (m). The diffractograms of commercial NiO and PdO are included for comparison.

narrow peaks (high crystallinity) at  $2\theta \approx 34, 42, 55, 60, 61^\circ$ , assignable to a tetragonal crystal system with  $\text{P4}_2/\text{mmc}$  space group (ICDD No. 04-004-5421). Bulk NiO and PdO are microcrystalline materials, with average crystallite size  $> 100\text{ nm}$  (Table 2).

The materials prepared exhibited a very broad peak in the range  $20\text{--}30^\circ 2\theta$  due to the amorphous nature of the pore walls of mesoporous materials of the type TUD-1 (Fig. 1). No crystalline phases could be distinguished in the PXRD patterns of NiTUD(10) and NiTUD(20), suggesting that these materials possessed isolated nickel sites, and/or

amorphous or distorted small metal nanoparticles. NiTUD(50) exhibited small peaks at  $2\theta \approx 37^\circ, 44^\circ$  assignable to nanocrystalline NiO (ICDD No. 04-013-0886), with average crystallite size of ca.  $5\text{ nm}$  (Fig. 1, Table 2). The small peaks of the crystalline phase were undistinguishable when the PXRD data was collected in less time (e.g. steps of  $0.026^\circ$ ). Excluding the materials prepared via the FW method and 1PdNiTUD(10), it was verified a slight increase of the average sizes of the NiO nanocrystallites after the impregnation of palladium. It seems that palladium impregnation was accompanied by some aggregation of nickel species, especially for the IWI method. All palladium-containing materials possessed PdO nanocrystallites with average sizes in the range  $2\text{--}12\text{ nm}$ , which were larger for those with  $y = 7$  than  $y = 1$  (Table 2).

The STEM images and Si and Ni mappings of NiTUD suggested uniform metal distributions (Figs. 2–4). For the bimetallic materials, it was verified dispersed Ni- and Pd-containing nanoparticles on the silicate matrix, with superimposable regions containing palladium and nickel, suggesting close proximity of the two metals. For monometallic 7PdTUD-1 it was not verified uniform palladium distribution (Fig. 4).

All materials prepared exhibited type IV nitrogen adsorption isotherms and a hysteresis loop associated with mesoporosity (Figs. 5, S2). The materials NiTUD(x) possessed  $S_{\text{BET}}$  in the range  $350\text{--}456\text{ m}^2\text{g}^{-1}$ , and mesopore sizes ( $D_p$ ) in the range  $12\text{--}32\text{ nm}$  (Table 1). The introduction of palladium did not influence drastically the textural properties of the parent materials NiTUD(x);  $S_{\text{BET}}$  decreased by factors in the range  $1.1\text{--}1.2$ , and the values of  $V_p$  were comparable. The materials prepared via the FW procedure possessed slightly higher  $S_{\text{BET}}$  and  $V_p$  than those prepared via the IWI method ( $x = 20$ ), which is consistent with the PXRD and STEM results in that the former method gave materials with relatively small, uniformly distributed metal species. The impregnation of palladium on the mesoporous silica TUD-1 ( $S_{\text{BET}} = 532\text{ m}^2\text{g}^{-1}$ ) gave 7PdTUD-1 with decreased  $S_{\text{BET}}$  (by a factor of  $\approx 1.3$ ), which may be partly due to less uniform distribution (based on STEM, Fig. 4) of relatively large PdO nanocrystallites (based on PXRD, Table 2) for this material.

The reduction properties were studied by TPR- $\text{H}_2$  analysis for the mono- and bimetallic TUD-1 type materials, and, for comparison, mesoporous silica TUD-1, and commercial bulk NiO and PdO (Fig. 6). TUD-1 did not exhibit  $\text{H}_2$  consumption, whereas the Ni- and/or Pd-containing materials did, indicating that the reduction properties are associated with the transition metal species. The monometallic palladium-containing materials PdO, 7PdTUD-1 and 7PdAlTUD-1 exhibited solely a negative TPR- $\text{H}_2$  peak in the low temperature range (up to  $\approx 120^\circ\text{C}$ ), and no significant  $\text{H}_2$  consumption at higher temperature. Based on literature data, the negative peak may be due to PdO species, which were converted to palladium hydride species ( $\beta$ -phase), under  $\text{H}_2$  atmosphere at relatively low temperature, prior to the TPR- $\text{H}_2$  analysis; during the analysis, the metal hydride species are decomposed giving  $\text{H}_2$ , which produces a negative response in the TCD detector [85,86].

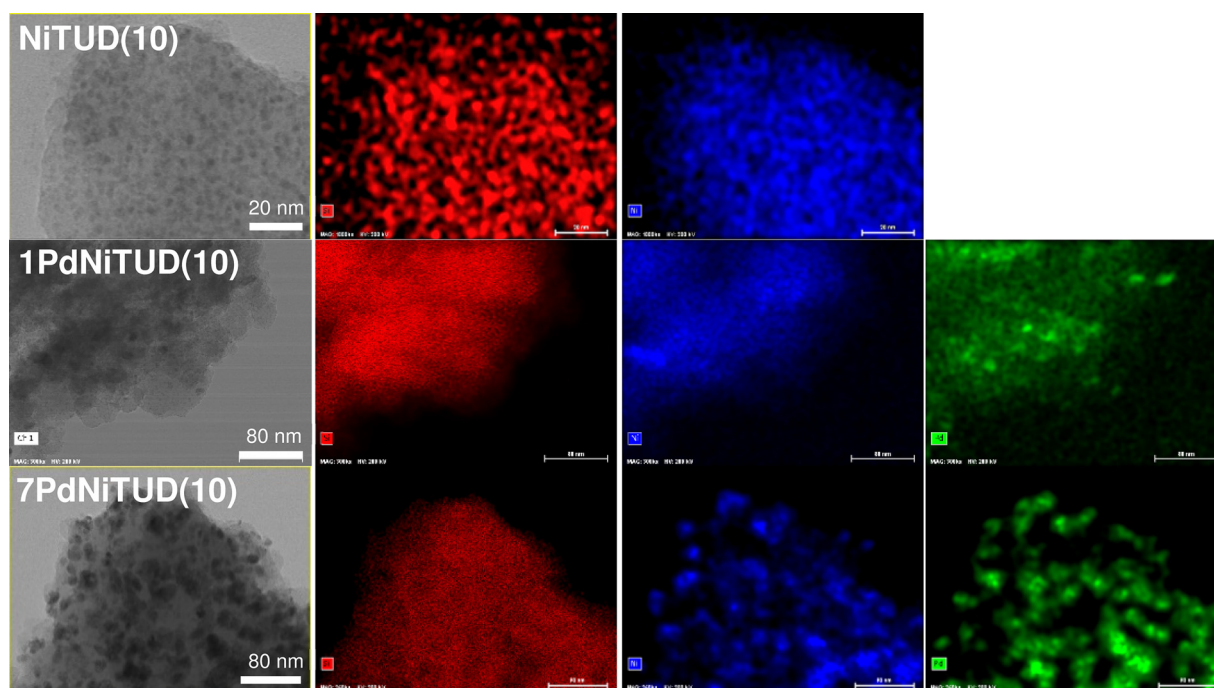
Bulk NiO exhibited  $\text{H}_2$  consumption essentially in two temperature ranges;  $\approx 250\text{--}550^\circ\text{C}$  and  $550\text{--}900^\circ\text{C}$ . The intermediate temperature reduction ( $\approx 250\text{--}550^\circ\text{C}$ ) may be related to non-stoichiometric oxygen in the bulk metal oxide, and Ni(II) to Ni(0) transition [87]. The higher temperature reduction may be a consequence of physical phenomena occurring during the reduction process and transformation of the bulk NiO. Specifically, surface metal nuclei may be formed via reaction between the oxide and  $\text{H}_2$ , leading to a metal cover that may eventually hinder diffusion of hydrogen to the interior of the crystals, and of oxygen in the opposite direction; these effects may be more pronounced for more crystalline (composition approximating stoichiometry) NiO, shifting the reduction peak to higher temperature [87,88].

The monometallic materials NiTUD(x) exhibited intermediate (up to  $\approx 480^\circ\text{C}$ ) and predominantly high temperature (above  $\approx 480^\circ\text{C}$ ) reduction, and no low temperature reduction (Fig. 6). A comparative study for the (monometallic) nickel versus palladium catalysts, indicates that the low temperature reduction is associated with palladium

**Table 2**

Average crystallites sizes, acid and reduction properties of the mono- and bimetallic TUD-1 type materials.

Sample	Average Crystallite size <sup>a</sup> (nm)		H <sub>2</sub> consumption (μmol g <sup>-1</sup> ), at T < 180 °C <sup>b</sup>	Lewis Acidity <sup>c</sup> (μmol g <sup>-1</sup> )		
	NiO	PdO		L <sub>150</sub>	L <sub>250</sub>	L <sub>250</sub> /L <sub>150</sub>
NiTUD(10)	nd <sup>d</sup>	–	–	159	78	0.5
1PdNiTUD(10)	nd <sup>d</sup>	5	14	93	40	0.4
7PdNiTUD(10)	9	9	44	89	50	0.6
NiTUD(20)	nd <sup>d</sup>	–	–	56	28	0.5
1PdNiTUD(20)	3	5	4	44	25	0.6
1PdNiTUD(20)w	nd <sup>d</sup>	2	19	56	38	0.7
7PdNiTUD(20)	9	12	72	26	17	0.7
7PdNiTUD(20)w	nd <sup>d</sup>	6	124	104	79	0.8
NiTUD(50)	5	–	–	20	5	0.3
1PdNiTUD(50)	8	6	25	13	6	0.5
7PdNiTUD(50)	12	6	50	14	5	0.4
7PdAlTUD-1	–	6	93	–	–	–
7PdTiTUD-1	–	10	135	4	2	0.5
NiO	> 100 <sup>e</sup>	–	–	–	–	–
PdO	–	> 100 <sup>e</sup>	2056	–	–	–

<sup>a</sup> Determined by PXRD.<sup>b</sup> Based on the integration of the TPR-H<sub>2</sub> curves below 120 °C (corresponding to the catalytic reaction temperature range used).<sup>c</sup> Based on FT-IR spectroscopy of adsorbed pyridine.<sup>d</sup> PXRD pattern with no distinguishable peaks of crystalline NiO or PdO.<sup>e</sup> The precise average crystallites sizes are not given because of the reduced reliability of the results for (micro)crystallite sizes greater than 100 nm.**Fig. 2.** STEM images of the TUD-1 type materials prepared from NiTUD(10), and the respective mappings of silicon (red), nickel (blue), and palladium (green). For each material, the scale is the same for all the corresponding images.

species, and the intermediate/high temperature reduction with nickel species. The high temperature reduction of the TUD-1 type materials may be due to nickel species strongly interacting with the silicate matrix, e.g. isolated or small ensembles of Ni(II) species on the surface or inside the pore walls; on the other hand, the intermediate temperature reduction may be due to larger ensembles (nanocrystallites) of NiO interacting less strongly with the support [81,89–91].

The TPR-H<sub>2</sub> profiles of the bimetallic materials were different from those of the parent materials NiTUD(x), especially for the materials with y = 7 prepared via the IWI method (Fig. 6). It is known from the literature that noble metals may influence the reducibility of metal oxides [92–94]. The bimetallic materials yPdNiTUD(x) (prepared via the IWI method) exhibited low (< 120 °C), intermediate (up to

≈ 480 °C) and high temperature (above ≈ 480 °C) reduction. The negative and positive peaks below 120 °C are assignable to the decomposition of palladium hydride species and the reduction of PdO species, respectively [89]. The intermediate temperature reduction seemed more pronounced for 7PdNiTUD(10) and 7PdNiTUD(20), which possessed relatively large NiO nanocrystallites (≈ 9 nm average size, Table 2), and these may interact less strongly with the support. The materials prepared via the FW procedure (yPdNiTUD(20)w) exhibited essentially low (palladium species) and high temperature reduction (strong nickel-support interactions), and no significant intermediate temperature reduction. These results together with PXRD and STEM, suggest that the FW procedure led to materials possessing relatively uniform distribution of nickel species (isolated sites or very small

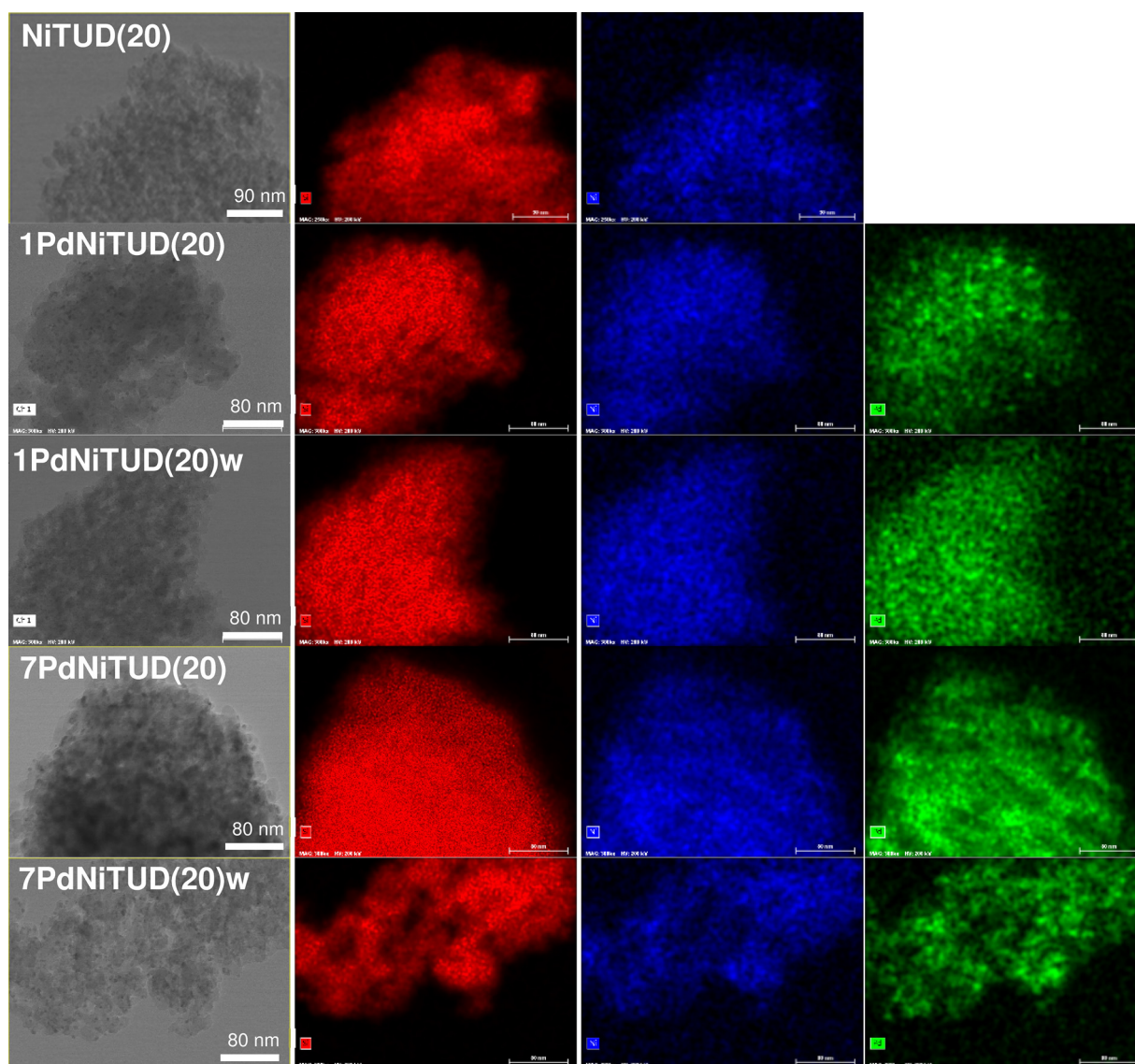


**Fig. 3.** STEM images of the TUD-1 type materials prepared from NiTUD(20), and the respective mappings of silicon (red), nickel (blue), and palladium (green). For each material, the scale is the same for all the corresponding images.

ensembles) strongly interacting with the mesoporous matrix, which are less prone to reduction.

Importantly, supported PdO species may be readily reduced at temperatures in the range of the catalytic tests ( $\leq 170^\circ\text{C}$ ), the reducing species are palladium-containing ones, and no reduced (or metallic) nickel is expected under the catalytic conditions (Table 2). The values of  $\text{H}_2$  consumption due to palladium species (based on the total area of the positive plus negative peaks) are given in Table 2 for rough comparisons with the catalytic results discussed ahead. It seemed that the reducibility was enhanced with increasing palladium content, and, on the other hand, for the materials prepared via the FW method. Nevertheless, care should be taken in the interpretation of these results due to the ease of palladium reduction at low temperature, prior to analysis, which may lead to more or less underestimated results.

The acid properties of the materials were measured by FT-IR spectroscopy using pyridine as base probe (Table 2). The materials possessed Lewis (L) acidity and no measurable Brønsted acidity. The NiTUD(x) materials exhibited a band at ca.  $3625\text{ cm}^{-1}$  before and after pyridine adsorption (not shown), which was not observed for PdTUD-1 (not shown), and may be due to “non-acidic” Ni-OH species [95,96]. A comparative study for the monometallic materials NiTUD(x) and

7PdTUD-1 suggested that the acidity was essentially due to nickel-containing species (Table 2). These results together with the TPR- $\text{H}_2$  studies, suggested that the nickel species furnish the material with acidity, whereas the palladium species account for the reduction properties, under the catalytic reaction conditions ( $140\text{--}170^\circ\text{C}$ ).

The amount of L acid sites of NiTUD(x) increased with decreasing Si/Ni ratio. NiTUD(x) possessed higher amount of L acid sites than the corresponding bimetallic materials yPdNiTUD(x) prepared via the IWI method, which may be a result of the enlarged NiO nanocrystallites after the introduction of palladium (Table 2, Fig. 1), reducing the amount of accessible acid sites. The FW procedure led to enhanced amount and strength of L acid sites (yPdNiTUD(20)w) in relation to the IWI method (yPdNiTUD(20)), which may be due to the relatively uniform distribution of nickel species in the former case. In general, the materials with x = 10 and 20 possessed mostly moderately strong Lewis acid sites ( $L_{250}/L_{150}$  in the range 0.4–0.8), and the materials with x = 50 possessed weaker acidity (0.3–0.5).

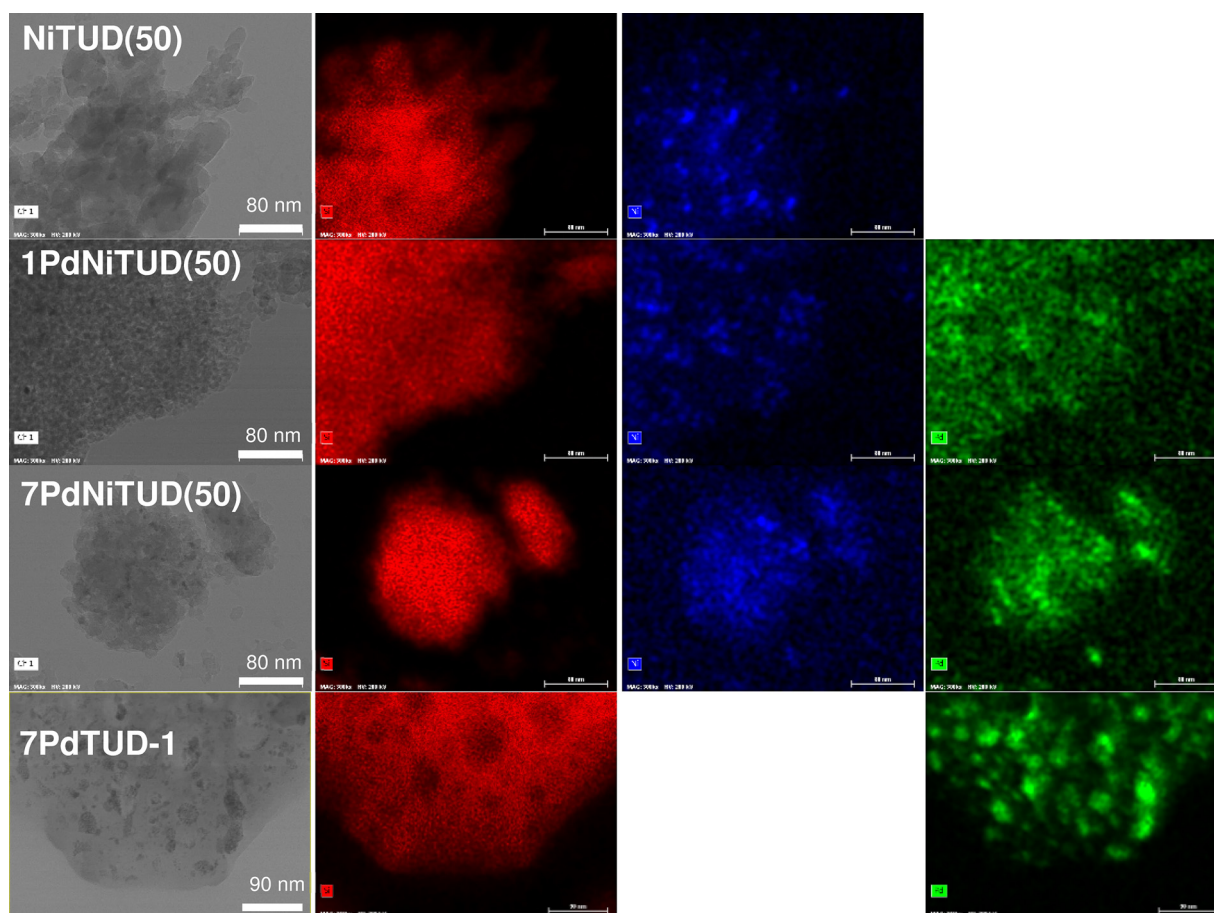


**Fig. 4.** STEM images of the TUD-1 type materials prepared from NiTUD(50), and PdNiTUD-1, and the respective mappings of silicon (red), nickel (blue), and palladium (green). For each material, the scale is the same for all the corresponding images.

### 3.2. Catalytic studies

#### 3.2.1. General considerations

The bimetallic Pd-Ni TUD-1 type mesoporous catalysts were active for the conversion of FUR, using formic acid (FAC) as hydrogen source, and ethanol or 1-butanol as reacting solvent (ROH = EtOH or BuOH, respectively), at 140 °C (Fig. 7a,b and S3a-h, Table 3). The bimetallic catalysts led to the bioproducts (bioPs) 2-alkoxyfurans (EoF, BoF), 2-methylfuran (2MF), 4-oxopentanal (OP) and its acetals (OPea, OPba). Total bioPs yield of up to 70% at 71% conversion were reached at 24 h, 140 °C (Fig. S3f). Detailed studies of the influence of material properties on the catalytic reaction and mechanistic considerations are discussed ahead.

Blank/control tests were carried out in order to assess the role of each component of the initial reaction mixture (FUR/FAC/EtOH/7PdNiTUD-1(10)) in the overall catalytic process; the results are discussed in detail in the ESI section (Fig. S4). In summary, the simultaneous presence of FAC and the catalyst was necessary to trigger FUR conversion to bioPs. The characterisation studies indicated that the supported palladium species may be readily reduced by H<sub>2</sub> at the catalytic reaction temperature. Palladium catalysts are known to be effective for H<sub>2</sub> production from FAC, under mild reaction conditions [61–63]. The reduced palladium species likely triggered the FUR conversion. The use of acetic acid [97–101] or ammonium formate [102,103] as hydrogen sources instead of FAC, did not give bioPs. Tan et al. [99] reported for a commercial palladium catalyst the effective H<sub>2</sub> production from FAC, but not from acetic acid; conversely, a commercial nickel oxide catalyst converted acetic acid to H<sub>2</sub>, albeit at very high temperature (300 °C). The characterisation studies of the bimetallic

TUD-type catalysts indicated that the reduction of nickel species required higher temperature than that used for the catalytic tests. Possibly, the poor results with acetic acid as H-carrier may be due to a higher thermal demand. The alcohol media favoured the selective conversion of FUR. Beneficial effects of alcohol media on reaction selectivity in relation to aqueous medium were reported in the literature for several reactions of biomass and derived chemicals [15,104–106].

Studies of the influence of the molar ratio FAC:FUR (in the range 22–65) on the catalytic reaction (at constant initial molar ratio EtOH:FUR = 51, or at constant total volume of reaction mixture and initial concentration of FUR; discussed in detail in the ESI section, Fig. S4) suggested that a reasonable compromise of the reaction conditions leading to reduced amounts of by-products seemed to be reached for FAC:FUR in the range 22–32, and EtOH:FUR in the range 44–51. Studies of the influence of the amount of catalyst on the FUR reaction (discussed in detail in the ESI section), suggested that a higher amount of catalyst accelerates simultaneously hydrogen formation in situ, and the formation of the bioPs.

For each catalyst 7PdNiTUD(x), using EtOH or BuOH as reacting solvent led to roughly comparable kinetic profiles (Fig. S5) and the initial catalytic activities were similar, at 140 °C (Table 3). The total bioPs yields (and overall selectivity) tended to be higher for BuOH than EtOH (Table 3). Increasing the reaction temperature of the system FUR/FAC/BuOH from 140 °C to 170 °C led to a considerable increase in FUR conversion and total bioPs yields (predominantly 2MF), at 7 h (Table 3, Fig. S3). These results may be due to a complex interplay of different factors. H<sub>2</sub> may be more soluble in BuOH than EtOH [107–109], and the solubility of H<sub>2</sub> in ROH may increase with increasing temperature. On the other hand, the solvent polarity is higher for EtOH than BuOH

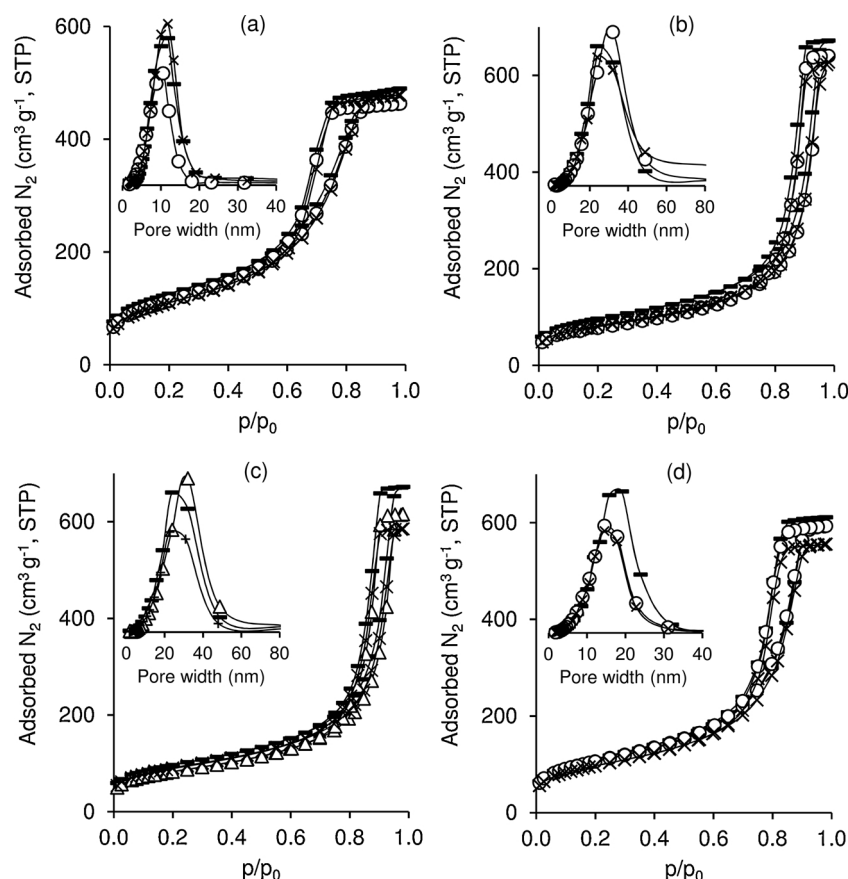


**Fig. 5.** Nitrogen adsorption-desorption isotherms, at  $-196^{\circ}\text{C}$ , of the materials NiTUD( $x$ ) (—), 1PdNiTUD( $x$ ) (o), 7PdNiTUD( $x$ ) ( $\times$ ) possessing  $x = 10$  (a),  $x = 20$  (b),  $x = 50$  (d), and for (c) 1PdNiTUD(20)w ( $\Delta$ ) and 7PdNiTUD(20)w ( $+$ ).

(dielectric constant ( $\epsilon$  at  $70^{\circ}\text{C}$ ) is 19.45 and 13.44, respectively [110]), which may lead to competitive adsorption effects of more or less polar reactants/intermediates/products, influencing product selectivity [111]. The reaction temperature may also alter the preferential reaction pathways (involving different activation energies).

The best-performing catalyst was 7PdNiTUD(20)w, which led to 83% 2MF yield at 98% FUR conversion, using BuOH, at  $170^{\circ}\text{C}$  (Fig. 7c and 8-g-h). Clear and fair comparisons to literature data for different catalysts are not trivial, being quite difficult due to different reaction conditions used between different studies. Considering the benefits of the catalytic protocol of the present work, specifically, no usage of high-pressure gas or externally supplied  $\text{H}_2$ , no need for stages of catalyst pre-reduction (typically with  $\text{H}_2$  at high temperature), and use of alcohol media to enhance product selectivity and reduce waste production, a literature search was performed based on these criteria for FUR conversion to 2MF. The literature survey indicated few studies in relation to the vast literature of processes involving externally supplied  $\text{H}_2$  for catalyst pre-reduction and/or the conversion of FUR. Very recently, Albonetti, Cavani and coworkers [112] studied the reaction of FUR with an organic H-source, at 1 atm, in the reaction temperature range  $250\text{--}400^{\circ}\text{C}$ , over a  $\text{FeVO}_4$  catalyst, under continuous-flow operation (C-F). An outstanding result was 55% 2MF yield, at 79% FUR conversion,  $320^{\circ}\text{C}$ , 1 atm, and using an aqueous solution of 37 wt%  $\text{CH}_2\text{O}$  plus 7–8 wt%  $\text{CH}_3\text{OH}$  [112]. At  $210^{\circ}\text{C}$ , Yang et al. [113] reported FUR reaction with FAc giving 79% 2MF yield over carbon supported with 22% Cu plus Ni, involving catalyst pre-reduction with externally supplied  $\text{H}_2$  at  $400^{\circ}\text{C}$ . At  $180^{\circ}\text{C}$ , Chang et al. [114] reported FUR reaction with 2-propanol over zirconia-supported Pd-Cu, giving ca. 65% 2MF yield, also involving catalyst pre-reduction with  $\text{H}_2$  at  $500^{\circ}\text{C}$ . The bimetallic TUD-1 type materials led to high 2MF yields at lower reaction temperature, without the need for catalyst pre-reduction stages.

Some studies involved the use of organic agents (formic acid, 2-propanol) for  $\text{H}_2$  supply in situ, and high pressure of  $\text{N}_2$  (10–21 bar) under batch conditions (using autoclaves), giving high 2MF yields, over noble or non-noble metal catalysts. Pressurising the systems may enhance the solubility of the product  $\text{H}_2$ , although it is more demanding in terms of equipment/operation costs. Specifically, Wang et al. [115] reported 83% 2MF yield for FUR conversion, using 2-propanol for  $\text{H}_2$  supply, over Ru-Ni- $\text{Fe}_2\text{O}_4$ , at  $180^{\circ}\text{C}$  and 21 bar  $\text{N}_2$ . At higher temperature of  $200\text{--}210^{\circ}\text{C}$  (10 bar  $\text{N}_2$ ), Fu et al. [116,117] reported 91–92% 2MF yield, over carbon or alumina-supported with 20 wt% Ni plus Cu, using FAc and 2-propanol as solvent; the catalysts were pre-treated with externally supplied  $\text{H}_2$  at  $550^{\circ}\text{C}$ . Catalyst pre-reduction stage and pressurising the reactors are avoided in the protocol of the present work. The catalysts' costs and productivities, and energy efficiency of the overall process are amongst several important factors that need to be contemplated for more realistic comparisons.

The literature for FUR-to-2MF conversion involving externally supplied  $\text{H}_2$  for the catalytic reduction is extremely vast, and has been addressed in some review articles [9,10,14,59], going from very recent research publications (year 2017) [118–127] to others published 50 or more years ago [128,129]. The  $\text{H}_2$  based process conditions go from batch to C-F, atmospheric to high pressure, using noble or non-noble catalysts, requiring or not a stage of catalyst pre-reduction with externally supplied  $\text{H}_2$  at higher temperature. Interesting systems involving noble metal catalysts with  $\text{H}_2$  under relatively mild temperature and pressure conditions, and without the need for catalyst pre-reduction stage were reported. Hutchings and co-workers [130] demonstrated how the catalyst Ru-Pd/ $\text{TiO}_2$  was capable of promoting FUR conversion to 2MF, which was formed with good selectivity ( $\approx 20\%$  yield, 39% conversion), outstandingly at room temperature and using  $\text{H}_2$  only slightly above atmospheric pressure (3 bar; octane as solvent).

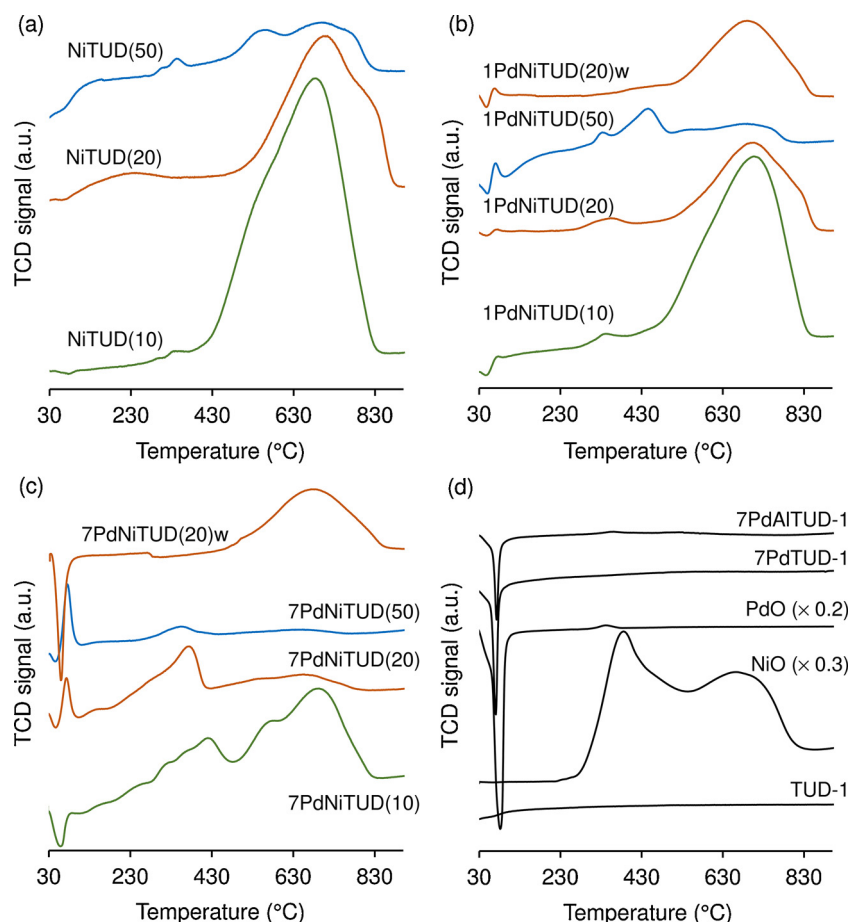


Fig. 6. TPR-H<sub>2</sub> profiles for the mono- and bimetallic TUD-1 type materials, and bulk PdO and NiO.

Recently, Dohade et al. [131] reported up to 59% 2MF yield over a Pt/Co/C catalyst, using relatively low H<sub>2</sub> pressure (5 bar), at 180 °C (isopropanol as solvent), under batch operation. At the same temperature (180 °C), albeit involving catalyst pre-reduction using H<sub>2</sub> at 500 °C, Wang et al. [132] reported 81% 2MF yield for the reaction system FUR/H<sub>2</sub>/1-propanol over 10 wt% impregnated PtCo<sub>3</sub>/C as catalyst, under C–F. 2MF yields above 80% were reported using non-noble metal catalysts under C–F, albeit with external supplied H<sub>2</sub>, at relatively high catalytic reaction temperature (200–300 °C), and requiring a catalyst pre-reduction stage with H<sub>2</sub> at high temperature [29,31–33,121,122,133–140]; all these factors are avoided in the present protocol.

Importantly, care should be taken in comparing different studies

solely based on a maximum reported value of 2MF yield. An example amongst many possible factors that may lead to erroneous conclusions is for C–F operation where the results should be considered under steady-state conditions, which is hardly specified or not the case. In a recently reported C–F protocol, at relatively high temperature (210 °C), and requiring catalyst pre-reduction (pure H<sub>2</sub> at 300 °C), it was reported the reaction of FUR with H<sub>2</sub> over mesoporous silica supported with 10 wt% Cu giving very high 2MF yield (> 95%) in the first few hours on-stream, although 2MF selectivity dropped considerably with time-on-stream (< 60% at 24 h) [121]. Some C–F systems use an organic solvent at high temperature, which requires some caution; e.g. cyclopentyl methyl ether [121] is considered a “green” solvent, albeit highly inflammable with an auto-ignition temperature (180 °C) below the

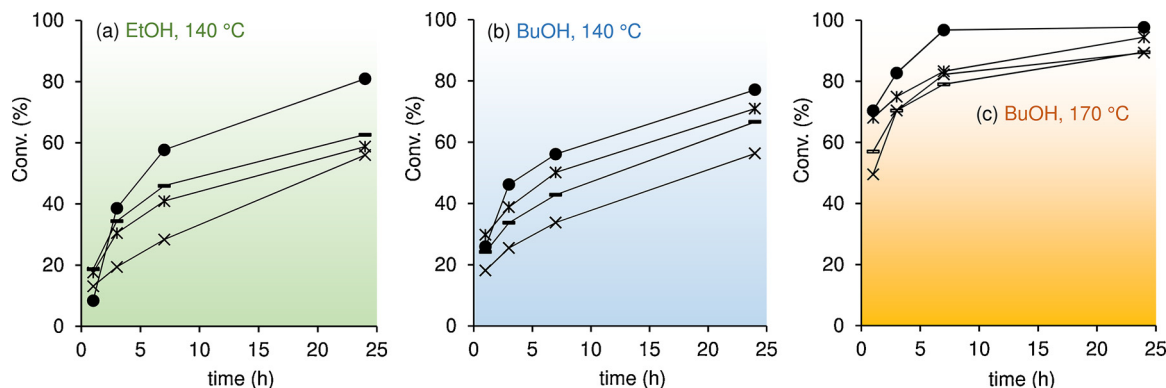


Fig. 7. Kinetic profiles of FUR reaction using (a) EtOH or (b) BuOH as solvent, at 140 °C, or (c) BuOH at 170 °C, in the presence of 7PdNiTUD(10) (○), 7PdNiTUD(20)w (●), 7PdNiTUD(50) (×) or 7PdNiTUD(20) (\*). Reaction conditions: [FUR]<sub>0</sub> = 0.26 M, catalyst load = 12.8 g L<sub>mix</sub><sup>−1</sup>.

**Table 3**Reaction of FUR, in the presence of the mono- or bimetallic catalysts 7PdNiTUD(x) and 7PdNiTUD(20)w, in alcohol (ROH) media<sup>a</sup>.

Catalyst	ROH	T (°C)	Initial activity (mmol g <sub>cat</sub> <sup>-1</sup> h <sup>-1</sup> )	Conv. (%)	Yields of bioPs (%)				
					AoF	OP	OP acetals	2MF	Total
7PdNiTUD(10)	EtOH	140	4	65	11	3	16	9	39
7PdNiTUD(20)	EtOH	140	4	59	9	2	17	11	39
7PdNiTUD(50)	EtOH	140	3	56	14	1	12	9	36
7PdNiTUD(20)w	EtOH	140	2	81	10	11	11	14	46
7PdNiTUD(10)	BuOH	140	5	67	24	13	17	11	64
7PdNiTUD(20)	BuOH	140	6	71	38	6	6	20	70
7PdNiTUD(50)	BuOH	140	4	56	34	3	2	15	54
7PdNiTUD(20)w	BuOH	140	5	77	24	14	7	17	61
7PdNiTUD(10)	BuOH	170	12	90	4	2	5	51	63
7PdNiTUD(20)	BuOH	170	14	94	1	3	9	53	66
7PdNiTUD(50)	BuOH	170	10	94	1	3	9	53	66
7PdNiTUD(20)w	BuOH	170	14	98	1	3	4	83	90

<sup>a</sup> Reaction conditions: [FUR]<sub>0</sub> = 0.26 M, catalyst load = 12.8 g L<sub>mix</sub><sup>-1</sup>, 24 h, 170 °C, 24 h.

temperature range generally reported for C–F protocols of FUR-to-2MF. A former study by Cui et al. [134] reported the use of  $\gamma$ -butyrolactone as renewable solvent at 190 °C, for the reaction of xylose-to-FUR-to-2MF, under C–F operation, using H<sub>2</sub> and solid mixtures of catalysts (zeolite Beta plus Cu–Zn–Al mixed oxides), giving 87% 2MF yield, but it should be considered the very high residence time (43.5 h; no mention to steady-state conditions) and the catalyst was pre-reduced with H<sub>2</sub> at 250 °C. However, this study importantly presents an integrated approach starting from the pentose [134]. Other recent studies of non-noble metal catalysts leading to high 2MF yields (> 80%), used harsh reaction conditions, i.e. high H<sub>2</sub> pressure and/or temperature, and a catalyst pre-reduction stage (H<sub>2</sub> at 450 °C) [119,126]. The above-mentioned studies are examples given in the literature for FUR conversion to 2MF, which is a topic of continuous investigation, partly motivated by the frequently identified catalyst stability issues.

The use of noble metal catalysts for the one-pot FUR conversion processes may present as benefits operating at relatively moderate reaction temperature and pressure conditions, less energy-intensive and safer processes, and good selectivities. On the other hand, although the reaction conditions used were not hydrothermal, water is a coproduct formed in the overall reaction. In mitigating catalyst deactivation in biomass conversion, Lange [58] reported that, in the presence of water, noble metal catalysts may present enhanced stability in relation to non-noble catalysts. The relevant role of noble metal catalysts in biomass conversion to chemicals/fuels was recently reviewed, highlighting commercial/pilot-scale projects by companies from America, Europe and Asia [59]. Concerns regarding the reduced availability of noble metals are being mitigated through different approaches, such as the one reported very recently by Opwis et al. [141] using functional textile materials as adsorbents, the feasibility of which was demonstrated for palladium-containing process waters of a producer in Germany.

### 3.2.2. Reaction mechanism and influence of material properties

In order to establish structure-activity relationships, it is important to understand the overall reaction mechanism. Hence, possible reaction intermediates were used as substrates (with FAc/EtOH/7PdNiTUD(10), 140 °C, Table 4). For the sake of simplicity, the bioPs formed from each substrate (S) are denoted bioP<sub>(S)</sub>.

Furfuryl alcohol (FA), which is a product of the hydrogenation of FUR, was formed in less than 1% yield in the catalytic reaction of FUR. With FA as substrate, the reaction was very fast (95% conversion at 1 h), giving EoF (8% yield), 2MF (10%) and OPea (7% at 24 h). EoF may be formed via the etherification of FA, and OPea via furan ring-opening, reduction, and acetalisation. The predominant OPea isomer was 5,5-diethoxy-2-pentanone; the other isomer, namely, 2,2-diethoxy-5-pentanal was always formed in less than 1% yield for all catalytic tests. FA was far more reactive than FUR (95% FA conversion at 1 h,

**Table 4**Reaction of different substrates (S), in the presence of 7PdNiTUD(10), in order to gain mechanistic insights<sup>a</sup>.

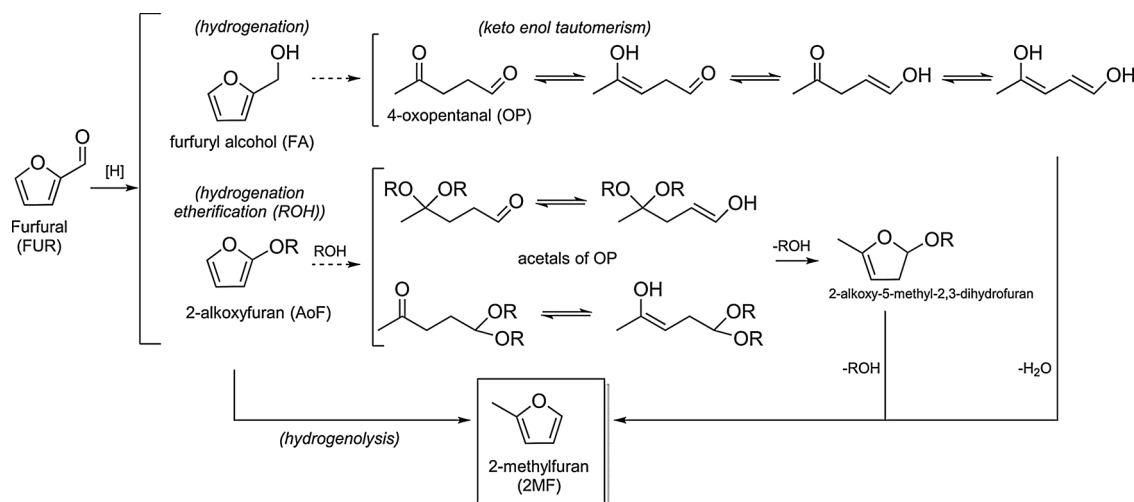
Substrate	Time (h)	Conv. (%)	Yield of bioP <sub>(S)</sub> (%)				Other products <sup>d</sup> (%)
			EoF	OP	OPdea	2MF	
FUR	24	65	11	3	16	9	–
FA	1	95	8	–	7	10	–
	7	99	16	–	15	10	–
EoF	7	41	–	–	10	7	EL (2)
	24	84	–	1	26	10	AnL(1), EL (8)
OP	7	66	–	–	50	1	–
	24 <sup>e</sup>	75	–	–	18	34	–
2MF	24	19	–	–	–	–	–
EL	24	23	–	–	–	–	–
AnL	1	85	–	–	50	–	EL (20), LA (28), GVL (2)
	7	100	–	–	–	1	EL (42), LA (37), GVL (8)

<sup>a</sup> Reaction conditions: [Substrate]<sub>0</sub> = 0.26 M, catalyst load = 12.8 g<sub>cat</sub> L<sub>mix</sub><sup>-1</sup>, EtOH, 140 °C.<sup>b</sup> Substrate (S) conversion.<sup>c</sup> Yield of the bioPs formed from the substrate (S).<sup>d</sup> The values in parenthesis are product yield (%).<sup>e</sup> BuOH at 170 °C was used instead of EtOH at 140 °C, and OPea was formed instead of OPea.

compared to 57% FUR conversion at 1 h). The higher reactivity of FA than FUR was also verified in aqueous medium, and no bioPs (100% FA decomposition at 1 h, compared to 45% FUR conversion at 24 h). These results suggest FA decomposition pathways in competition with those leading to the bioPs.

With EoF as substrate, 2MF and OPea were formed in 10% and 26% yield, respectively, at 84% EoF conversion, 24 h (Table 4). Hence, the formation of OPea and 2MF from FUR may involve the intermediate formation of EoF (Scheme 2). Somewhat consistent with this mechanistic proposal, the bioPs yields versus FUR conversion profiles showed that EoF yield reached a maximum, and then decreased with the concomitant formation of OPea and 2MF (Fig. S3). EoF was much less reactive (41% conversion at 7 h) than FA (95% conversion at 1 h), which is consistent with the faster FA conversion than bioP<sub>(FA)</sub> formation (the total bioP<sub>(FA)</sub> yield increased from 25% to 41%, at 95–99% FA conversion), Table 4.

Other products of EoF conversion included  $\alpha$ -angelica lactone (AnL) and ethyl levulinate (EL), although these products were not formed from FUR (at least not to measurable amounts), suggesting that they are not important intermediates (Table 4). This hypothesis was further supported by the fact that: (i) with AnL as substrate, it was formed EL, levulinic acid (LA) and gamma-valerolactone (GVL), which were not



**Scheme 2.** Mechanistic proposal for the conversion of FUR to bioPs, using FAc as H-source, in the presence of the bimetallic Pd-Ni TUD-1 type mesoporous catalysts, in alcohol medium.

formed from FUR; (ii) with EL as substrate, no bioPs were formed; and (iii) OPea and 2MF were formed from FUR, and not from AnL or EL.

With OP as substrate, it was essentially formed OPea (50% yield at 66% conversion, 7 h) via acetalisation reaction, and 2MF was formed in 1% yield. At higher reaction temperature of 170 °C and using BuOH as solvent, it was formed 18% yield OPba and 34% 2MF, at 75% OP conversion, 24 h. Hence, OP and/or its acetals are possible intermediates of the conversion of FUR to 2MF, and this pathway seemed favoured at higher temperature (Scheme 2). OP and its acetals may undergo (acid-catalysed) keto-enol tautomerism followed by ring-closure leading to 2MF (Scheme 2). It was reported in the literature that OP may be formed from 2MF via acid-catalysed hydrolysis (involving furan ring-opening, and keto-enol tautomerism) [6,7,23,41], or from LA (via hydrogenation/dehydration) [44,45]. These pathways seem unlikely to occur under the reaction conditions used in this work. With 2MF as substrate, the reaction was very sluggish, and no bioPs were formed, indicating that it is a stable (end) product.

The overall reaction mechanism may involve the pathways FUR-FA-EoF(OP, OPea)-2MF (Scheme 2). 2MF may also be formed from FA/EoF via (C–O) hydrogenolysis, without the intermediate formation of OP/OPea [9,91,111,130,142]. It was reported in the literature that FA de-etherification may be favoured at higher temperature [111]; accordingly, the direct FA hydrogenolysis pathway may be favoured using BuOH, at 170 °C.

Table S1 compares the catalytic results for monometallic NiTUD(x), 7PdTUD-1, PdO, NiO, the synthesis precursors Ni(NO<sub>3</sub>)<sub>2</sub> and Pd(NO<sub>3</sub>)<sub>2</sub>, and bimetallic 7PdNiTUD(10) (EtOH, 140 °C). The FUR reaction was very sluggish for all monometallic nickel-containing catalysts and mesoporous silica TUD-1 (less than 11% conversion at 24 h, and no bioPs were formed). The characterisation studies indicated that NiTUD(x) were essentially Lewis acids under the catalytic reaction conditions. The ineffectiveness of NiTUD(x) for FUR conversion is consistent with the above mechanistic proposal in that FUR is firstly hydrogenated, for which the nickel species lack activity. The TPR-H<sub>2</sub> studies of the bimetallic catalysts indicated that higher temperatures are needed for the reduction of the nickel species.

The monometallic palladium catalysts led to superior catalytic results (38–54 % FUR conversion at 24 h, and 5–20 % bioPs yields) than the monometallic nickel ones, supporting the above hypothesis that FUR conversion is triggered in the presence of palladium species (plus FAc). 7PdTUD-1 led mainly to EoF, indicating that the (poor) acid properties of this material (Table 2) were sufficient to enable FA etherification. Pham et al. [143] reported the reaction of 2-methylpentanal with H<sub>2</sub>, over silica-supported palladium catalysts, at 125 °C,

and verified that etherification reaction required ensembles of palladium atoms (catalysts with higher metal loadings) which allowed the proximity of two modes involved, namely dicoordinated aldehyde <sup>2</sup> $\eta$ -(C,O) and alkoxide (<sup>1</sup> $\eta$ -(C)) species. Accordingly, and knowing that the TUD-1 type catalysts possess palladium nanocrystallites, it is possible that a similar mechanism may lead to FA etherification.

The bimetallic catalysts possessed superior performances to the monometallic ones (Table S1). Palladium supported on the mesoporous aluminosilicate Al-TUD-1 (7PdAlTUD-1) led to sluggish FUR reaction (19% conversion at 24 h). The coexistence of palladium and nickel species was favourable for enhancing the bioPs yields. This hypothesis was somewhat supported by the fact that a mechanical mixture of NiTUD(10) plus PdO (in mass amounts equivalent to those of Pd and Ni added together with the catalyst 7PdNiTUD(10)) led to lower FUR conversion and bioPs yield than the bimetallic catalyst; 39% bioPs yield (65% conversion) for 7PdNiTUD(10), and 17% bioPs yield for PdO + NiTUD(10) (41% conversion), at 24 h. Favourable effects between electronegative noble metals and oxophilic transition metals were reported for the hydrogenation of FUR to FA using high-pressure H<sub>2</sub>; specifically, Pt dissociated H<sub>2</sub>, and Co stabilised intermediates [131,144]. Theoretical and experimental characterisation studies reported in the literature, suggested that the aldehyde group of the reacting molecule may interact with Group VIII metals via di-coordinated <sup>2</sup> $\eta$ -(C,O) configuration (carbonyl group parallel to the catalyst surface) [86,91,145–147].

Based on the characterisation and catalytic studies, the palladium species are necessary for the reduction steps (e.g. hydrogenation, hydrogenolysis) and the nickel sites favoured the acid-catalysed steps (e.g. etherification, acetalisation). Although the materials did not possess Brønsted (B) acidity, one cannot rule out the hypothesis that B acidity is generated in situ via the polarisation of water molecules interacting with Lewis acid sites (water is a co-product of steps such as FA etherification, Scheme 2).

The influence of the palladium and nickel contents of the catalysts yPdNiTUD(x) on the reaction of FUR, was investigated, using EtOH or BuOH (Fig. 8), at 140 °C. The catalysts with y = 7 led to superior catalytic results than those with y = 1, suggesting that higher Pd loading favoured the FUR conversion to bioPs. Since the palladium species are responsible for initialising FAc conversion to hydrogen, and the FUR conversion to bioPs, one may expect that higher palladium loadings will accelerate the overall process. The Si/Ni ratio (x) of the bimetallic catalysts influenced the total bioPs yields, which was more pronounced for y = 7 than y = 1 (Fig. 8). For yPdNiTUD(x) with y = 7 (EtOH as solvent), the FUR conversion and bioPs yields at 7 h increased with

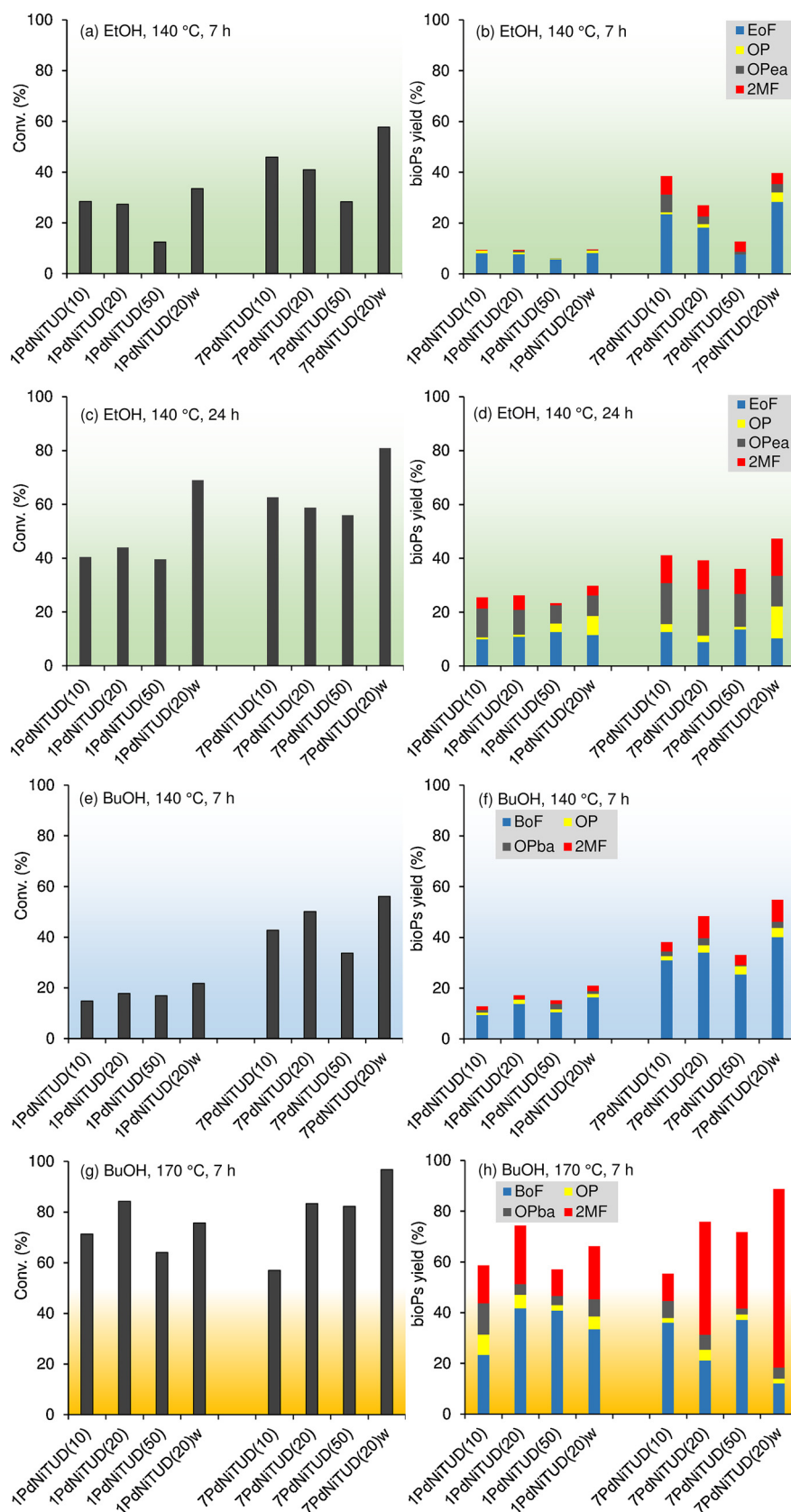


**Fig. 8.** Catalytic performance of the bimetallic catalysts on FUR conversion (a,c,e,g) and bioPs yields (b,c,f,h), using EtOH at 140 °C, 7 h (a,b), EtOH at 140 °C, 24 h (c,d), or BuOH at 140 °C, 7 h (e,f), BuOH at 170 °C, 7 h (g,h).

decreasing ratio Si/Ni ( $x$ ), which correlated with the increasing acidity of the catalysts. Enhanced catalyst acidity may favour reactions such as etherification and acetalisation. Conversely, in BuOH medium, the bimetallic catalysts possessing  $x = 20$  led to superior catalytic results, which did not correlate at least solely with the acid properties (Fig. 8, Table 2). Bulkier bioPs are formed with BuOH (BoF, OPba) than with EtOH (EoF, OPea), and thus steric effects may be more important in the former case. In this sense, the textural properties of 7PdNiTUD(20), which possessed the largest pores (Table 1), seemed favourable for FUR conversion to bioPs, in BuOH.

A comparative study for the materials prepared via the IWI or FW procedures and possessing  $x = 20$  and  $y = 7$ , indicated that, in general, the FW procedure led to superior catalytic results in terms of FUR conversion and bioPs yields at 7 h (Fig. 8). These results correlate with the apparently enhanced reducibility and acidity of the materials prepared via the FW procedure than the IWI method.

### 3.2.3. Catalyst stability

While the hydrothermal stability of various types of materials is being extensively investigated in the literature for biomass conversion processes, less attention is given to the solvothermal stability of catalytic materials for reactions of biomass in organic (polar, coordination) media, which are being increasingly considered for selectively targeting bioproducts [58]. The solvothermal stability is a very important aspect from a practical point of view.

The stability of the bimetallic TUD-1 type catalysts was studied by combining catalytic and characterisation studies. In particular, the solvothermal stability was studied by carrying out a contact test (CT) where the material was put into contact with the hot solvent without substrate (details in the experimental section). The liquid phase obtained from the CT for 7PdNiTUD(10) was transferred to a separate reactor, to which FUR and FAc were added, and the resultant homogeneous mixture (FUR/FAc/EtOH) was left to react, at 140 °C, with stirring. No conversion to bioPs occurred within 24 h (Fig. 9), suggesting the absence of soluble active metal species, and thus no metal

leaching from the material. ICP-AES indicated negligible amount of Pd in solution (detection limit  $\approx 20$  ppb), and a very small amount of nickel which corresponded to less than 2% Ni leaching. The solid obtained from the CT was tested for the FUR/FAc/EtOH reaction, and led to comparable catalytic results to the original catalyst (Fig. 9a,b). These results suggest good solvothermal stability of the bimetallic catalyst. The catalyst was reused for three consecutive batch runs, and led to comparable FUR conversion and bioPs yields (Fig. 9a,b). Likewise, the reused catalyst 7PdNiTUD(20)w was also stable in recycling runs (Fig. 9c,d). The used catalysts were characterised by PXRD, STEM, ICP-AES,  $N_2$  adsorption, and TPR- $H_2$ . In general, the compositions of the materials were comparable before and after use (Table S2). The low-angle XRD patterns of the original and corresponding used catalysts exhibited similar features associated with the mesoporosity (Fig. S1). The wide-angle XRD patterns of the recovered catalysts indicated that the average sizes of the metal nanocrystallites increased, especially for  $x = 10$  or 20 (Fig. S6, Table S3). In particular, the STEM images of the used catalyst 7PdNiTUD(10) suggested somewhat less uniform distribution of palladium (Fig. S7). The  $S_{BET}$  of the catalysts decreased after use, which may be partly due to the enlarged metal crystallites (Table S2).

The TPR- $H_2$  profiles indicated that all used catalysts exhibited low temperature reduction associated with palladium species, similar to that verified for the original catalysts (Fig. S8). The similar reduction properties associated with the palladium species correlated with the similar catalytic results for the original and used catalysts (7PdNiTUD(10), 7PdNiTUD(20)w). The  $H_2$  consumption associated with the palladium species did not decrease after use (Table S3); the values were higher which may be due to some uncertainty in the quantification of  $H_2$  consumption, as discussed above (Section 3.1). The TPR- $H_2$  profiles in the intermediate/high temperature ranges were different for the used and corresponding original materials (Fig. S8). Specifically, all used catalysts exhibited essentially intermediate temperature reduction, which may be associated with the enlarged NiO nanocrystallites (Table S3).

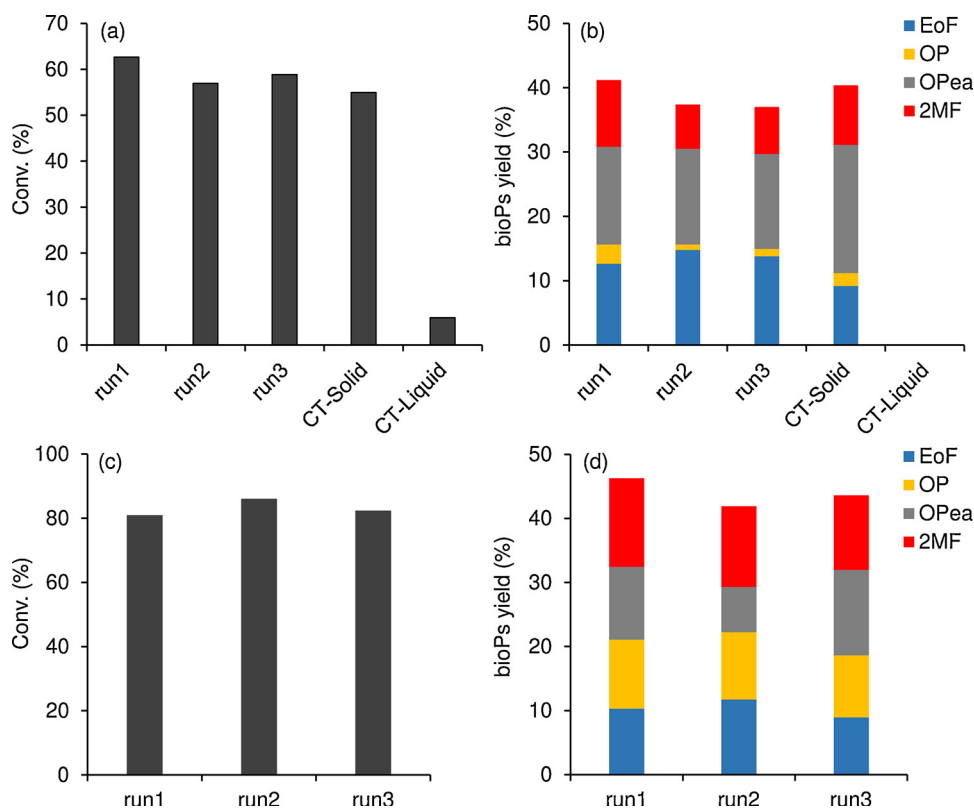


Fig. 9. FUR conversion (a, c) and yields of bioPs (b, d) for three consecutive 24 h batch runs of FUR reaction, in the presence of 7PdNiTUD(10) (a, b) or 7PdNiTUD(20)w (c, d), at 140 °C (molar ratio FAc:FUR = 22; EtOH:FUR = 51). The catalytic results for the liquid and solid phases obtained from the contact test (CT) using 7PdNiTUD(10) are given in (a) and (b).

The changes in nanocrystallite average sizes did not seem to affect the catalytic performance of the reused catalysts. Possibly, the catalyst surface properties changed in the reaction medium (during the catalytic reaction). The PXRD pattern of the used catalyst 7PdNiTUD(10) without any thermal treatment (denoted 7PdNiTUD(10)\*) was very different from those of the original and thermally regenerated (7PdNiTUD(10)-used) solids (Fig. S6f-h). The solid 7PdNiTUD(10)\* did not exhibit peaks of nanocrystalline PdO and NiO, and instead exhibited peaks at ca. 40 and 47° assignable to the (111) and (200) crystal planes of metallic Pd (Fig. S6h) [148,149]. No metallic Ni crystalline phases could be distinguished for 7PdNiTUD(10)\*, which is consistent with the characterisation studies in that the reduction of nickel required higher temperature than the catalytic reaction temperature. The above results suggested that the average sizes and distributions of metal species changed *in situ* during the catalytic reaction, as well as the type of palladium species. The FUR reaction in the presence of 7PdNiTUD(10)\* led to poorer catalytic results (11% total bioPs yield, predominantly EoF (6% yield), at 24 h, 140 °C) than 7PdNiTUD(10) and 7PdNiTUD(10)-used. Hence, the metal oxide surface species play important catalytic roles. Under atmospheric air and heating, metallic Pd is converted to PdO (ascertained by PXRD), which together with FAc is required for the *in situ* hydrogen supply, and the reduction steps of the overall catalytic process. Advantageously, no externally supplied H<sub>2</sub> is required, neither for catalyst pre-reduction nor for the catalytic conversion of FUR.

#### 4. Conclusions

Furfural (FUR) may be converted to the useful bioproducts 2-alkoxyfurans (AoFs), 2-methylfuran (2MF), 4-oxopentanal (OP) and its acetals, in the presence of bimetallic Pd-Ni TUD-1 type mesoporous catalysts, using formic acid (FAc) as *in situ* H-supplier, at 140–170 °C, in alcohol medium. The catalysts were synthesised in stepwise fashions, using different procedures and conditions. The nickel species were introduced during the hydrothermal synthesis of mesoporous TUD-1 type matrix, giving the nickel silicates NiTUD(x) with uniform distributions of nickel species, which furnished the materials with acid properties. Subsequently, palladium was supported in different fashions on NiTUD(x), furnishing the materials with reduction properties, making them multifunctional. The materials yPdNiTUD(x) (x and y related to the Ni and Pd contents, respectively) were prepared via incipient wetness impregnation-solvent evaporation-calcination (IWI), and yPdTUD(20)w via impregnation-filtration-washing-calcination (FW). The catalyst preparation method and conditions influenced the materials properties, and consequently the catalytic performance, based on detailed characterisation (microstructural/molecular level) and catalytic studies. The bimetallic materials possessed PdO nanocrystallites, and in some cases NiO nanocrystallites. The FW procedure allowed enhanced metal distributions even for materials with higher metal contents (which was not the case for the IWI method). Increasing the nickel and palladium content enhanced the acid (based on spectroscopic analysis using pyridine as base probe) and reduction properties (based on H<sub>2</sub> consumption up to the catalytic reaction temperature), respectively, and, in general, the catalytic performances improved. Nevertheless, when targeting bioproducts using bulkier alcohol (reacting) solvents, the textural properties (pore sizes) seem important besides the acid-reduction properties of the catalysts.

The reaction conditions influenced the catalytic reaction, e.g. water as solvent and large excess of FAc had detrimental effects on the formation of the bioPs. The best-performing catalyst was 7PdNiTUD(20)w, which led to 83% 2MF yield, at 98% FUR conversion (90% total bioPs yield), using 1-butanol as solvent at 170 °C, and exhibited steady catalytic performance in recycling runs. Mechanistic studies indicated the possible intermediate formation of 4-oxopentanal (and related acetals) in the conversion of FUR to 2MF; to the best of our knowledge, this has not been reported previously. The material surface properties change in

the reaction medium; metallic Pd surface species are formed and may be thermally converted (under atmospheric air) to PdO, which plays multiple roles in the overall catalytic process, such as *in situ* hydrogen supply from FAc, and enabling reduction pathways leading to the bioPs.

This protocol advantageously excludes the need for external usage of H<sub>2</sub> for catalyst pre-reduction stages or for the catalytic reaction of FUR, and allows operation under relatively moderate conditions. Moreover, FAc presents low toxicity, it is easy to handle/store, and a coproduct of carbohydrate biomass conversion processes, and thus its repurposing is highly desirable.

#### Acknowledgements

This work was developed in the scope of the project (Associate Laboratory) CICECO Aveiro Institute of Materials-POCI-01-0145-FEDER-007679 [FCT (Fundação para a Ciência e a Tecnologia) ref. UID/CTM/50011/2013], financed by national funds through the FCT/MEC and when applicable co-financed by FEDER (Fundo Europeu de Desenvolvimento Regional) under the PT2020 Partnership Agreement. The FCT and the European Union are acknowledged for post-doctoral grants to M.M.A. (SFRH/BPD/89068/2012) and A.F. (SFRH/BPD/91397/2012), co-funded by MCTES and the European Social Fund through the program POPH of QREN. S.L., K.H. and D.C. thank EPSRC(UK) for financial support under EP/K014749/1. The authors are grateful to Dr. Rosário Soares (CICECO) for the assistance in the powder XRD measurements.

#### Appendix A. Supplementary data

Supplementary material related to this article can be found, in the online version, at doi:<https://doi.org/10.1016/j.apcatb.2018.06.004>.

#### References

- [1] K.J. Zeitsch, *The Chemistry and Technology of Furfural and Its Many by-Products*, 1st ed., Elsevier Science B. V., Amsterdam, The Netherlands, 2000.
- [2] G.V. Research, Global Furfural Market by Application (Furfuryl Alcohol, Solvents) Expected to Reach USD 1,200.9 Million by 2020, (2008) (Accessed 3 February 2018), <https://www.grandviewresearch.com/pressrelease/global-furfural-market>.
- [3] A.S. Mamman, J.-M. Lee, Y.-C. Kim, I.T. Hwang, N.-J. Park, Y.K. Hwang, J.-S. Chang, J.-S. Hwang, *Biofuels Bioprod. Biorefin.* 2 (2008) 438–454.
- [4] P. Bhaumik, P.L. Dhepe, *Catal. Rev.* 58 (2016) 36–112.
- [5] P. Zhou, Z. Zhang, *Catal. Sci. Technol.* 6 (2016) 3694–3712.
- [6] M.J. Climent, A. Corma, S. Iborra, *Green Chem.* 16 (2014) 516–547.
- [7] J.-P. Lange, E. van der Heide, J. van Buijtenen, R. Price, *ChemSusChem* 5 (2012) 150–166.
- [8] S. Dutta, S. De, B. Saha, M.I. Alam, *Catal. Sci. Technol.* 2 (2012) 2025–2036.
- [9] R. Mariscal, P. Maireles-Torres, M. Ojeda, I. Sadaba, M. Lopez Granados, *Energy Environ. Sci.* 9 (2016) 1144–1189.
- [10] K. Yan, G. Wu, T. Lafleur, C. Jarvis, *Renew. Sustain. Energy Rev.* 38 (2014) 663–676.
- [11] B. Liu, Z. Zhang, *ChemSusChem* 9 (2016) 2015–2036.
- [12] M.J. Gilkey, B. Xu, *ACS Catal.* 6 (2016) 1420–1436.
- [13] X. Li, P. Jia, T. Wang, *ACS Catal.* 6 (2016) 7621–7640.
- [14] L. Hu, G. Zhao, W. Hao, X. Tang, Y. Sun, L. Lin, S. Liu, *RSC Adv.* 2 (2012) 11184–11206.
- [15] S. Zhu, J. Guo, X. Wang, J. Wang, W. Fan, *ChemSusChem* 10 (2017) 2547–2559.
- [16] D.M. Alonso, S.G. Wettstein, J.A. Dumesic, *Green Chem.* 15 (2013) 584–595.
- [17] A. Osatiashtiani, A.F. Lee, K. Wilson, *J. Chem. Technol. Biot.* 92 (2017) 1125–1135.
- [18] I. Delidovich, K. Leonhard, R. Palkovits, *Energy Environ. Sci.* 7 (2014) 2803–2830.
- [19] P. Mäki-Arvela, B. Holmbom, T. Salmi, D.Y. Murzin, *Catal. Rev.* 49 (2007) 197–340.
- [20] M.H. Schneider, J.C. Phillips, *Furfuryl Alcohol and Lignin Adhesive Composition*, US 6747076 B2 (2004).
- [21] J.A.N.P.S. Watson, D.B. Rohr, D.E. Newquist, C.T. Crawford, L.W. Bragg, *Furfuryl Alcohol from China, South Africa, and Thailand*, U. S. International Trade Commission, Washington DC, USA, 1994.
- [22] D. Sun, S. Sato, W. Ueda, A. Primo, H. Garcia, A. Corma, *Green Chem.* 18 (2016) 2579–2597.
- [23] H. Li, S. Yang, A. Riisager, A. Pandey, R.S. Sangwan, S. Saravanamurugan, R. Luque, *Green Chem.* 18 (2016) 5701–5735.
- [24] A. Gandini, M.N. Belgacem, *Prog. Polym. Sci.* 22 (1997) 1203–1379.
- [25] Y. Nakagawa, M. Tamura, K. Tomishige, *ACS Catal.* 3 (2013) 2655–2668.
- [26] Y. Nakagawa, M. Tamura, K. Tomishige, *J. Jpn. Petrol. Inst.* 60 (2017) 1–9.

- [27] B. Vanderhaegen, H. Neven, L. Daenen, K.J. Verstrepen, H. Verachtert, G. Derdelinckx, *J. Agric. Food Chem.* 52 (2004) 1661–1668.
- [28] AROXATH, 2-Furfuryl Ethyl Ether, (2014) (consulted 5 October 2014), <http://www.aroxa.com/discovery/discoverystandard/-furfuryl-ethyl-ether/>.
- [29] Y.-L. Zhu, H.-W. Xiang, Y.-W. Li, H. Jiao, G.-S. Wu, B. Zhong, G.-Q. Guo, *N. J. Chem.* 27 (2003) 208–210.
- [30] A. Bohre, S. Dutta, B. Saha, M.M. Abu-Omar, *ACS Sustain. Chem. Eng.* 3 (2015) 1263–1277.
- [31] H.-Y. Zheng, Y.-L. Zhu, B.-T. Teng, Z.-Q. Bai, C.-H. Zhang, H.-W. Xiang, Y.-W. Li, *J. Mol. Catal. A Chem.* 246 (2006) 18–23.
- [32] J. Yang, H.-Y. Zheng, Y.-L. Zhu, G.-W. Zhao, C.-H. Zhang, B.-T. Teng, H.-W. Xiang, Y. Li, *Catal. Commun.* 5 (2004) 505–510.
- [33] H.-Y. Zheng, J. Yang, Y.-L. Zhu, G.-W. Zhao, *React. Kinet. Catal. Lett.* 82 (2004) 263–269.
- [34] H. Li, Q. Zhang, P. Bhadury, S. Yang, *Curr. Org. Chem.* 18 (2014) 547–597.
- [35] G.J.M. Gruter, 5-Substituted 2-(Alkoxyethyl)Furans, EP2487170 A1, (2012).
- [36] A.J.J.E. Eerhart, W.J.J. Huijgen, R.J.H. Grisel, J.C. van der Waal, E. de Jong, A. de Sousa Dias, A.P.C. Faaij, M.K. Patel, *RSC Adv.* 4 (2014) 3536–3549.
- [37] R.J. Haan, J.P. Lange, Gasoline Composition and Process for the Preparation of Alkylfurfuryl Ether, US 8372164 B2 (2013).
- [38] R.J. Haan, J.P. Lange, Gasoline Composition and Process for the Preparation of Alkylfurfuryl Ether, WO 2009077606 A2, (2009).
- [39] R.J. Haan, J. Lange, Gasoline Composition and Process for the Preparation of Alkylfurfuryl Ether, US 20110035991 A1, (2011).
- [40] C. Wang, H. Xu, R. Daniel, A. Ghafourian, J.M. Herreros, S. Shuai, X. Ma, *Fuel* 103 (2013) 200–211.
- [41] A. Corma, A.O. de la Torre, M. Renz, N. Villandier, *Angew. Chem. Int. Ed.* 50 (2011) 2375–2378.
- [42] C.A. Corma, M. Renz, A.O. de la Torre, Production of Liquid Fuels (Sylvan Liquid Fuels) from 2-Methylfuran, EP 2514802 A1, (2012).
- [43] G. Li, N. Li, J. Yang, L. Li, A. Wang, X. Wang, Y. Cong, T. Zhang, *Green Chem.* 16 (2014) 594–599.
- [44] D. Albani, Q. Li, G. Vile, S. Mitchell, N. Almora-Barrios, P.T. Witte, N. Lopez, J. Perez-Ramirez, *Green Chem.* 19 (2017) 2361–2370.
- [45] V.V. Ordonsky, J.C. Schouten, J. van der Schaaf, T.A. Nijhuis, *Appl. Catal. A Gen.* 451 (2013) 6–13.
- [46] X.-L. Du, Q.-Y. Bi, Y.-M. Liu, Y. Cao, H.-Y. He, K.-N. Fan, *Green Chem.* 14 (2012) 935–939.
- [47] E. Bertele, P. Schudel, Process for Preparation of Terpene Flavorants and Novel Intermediates Thereof, US 3872172 A, (1975).
- [48] E. Bertele, P. Schudel, Terpene flavorant intermediates, US 3962283 A (1976).
- [49] W.-M. Xiong, Y. Fu, F.-X. Zeng, Q.-X. Guo, *Fuel Process. Technol.* 92 (2011) 1599–1605.
- [50] M. Grasmann, G. Laurenczy, *Energy Environ. Sci.* 5 (2012) 8171–8181.
- [51] F. Joó, *ChemSusChem* 1 (2008) 805–808.
- [52] M.E.M. Berger, D. Assenbaum, N. Taccardi, E. Spiecker, P. Wasserscheid, *Green Chem.* 13 (2011) 1411–1415.
- [53] P. Zhou, Z. Zhang, L. Jiang, C. Yu, K. Lv, J. Sun, S. Wang, *Appl. Catal. B Environ.* 210 (2017) 522–532.
- [54] J. Albert, A. Jess, C. Kern, F. Pöhlmann, K. Glowienka, P. Wasserscheid, *ACS Sustain. Chem. Eng.* 4 (2016) 5078–5086.
- [55] F. Jin, J. Yun, G. Li, A. Kishita, K. Tohji, H. Enomoto, *Green Chem.* 10 (2008) 612–615.
- [56] K. Mandal, D. Bhattacharjee, S. Dasgupta, *Int. J. Hydrogen Energy* 40 (2015) 4786–4793.
- [57] H.H. Khoo, W.L. Ee, V. Isoni, *Green Chem.* 18 (2016) 1912–1922.
- [58] J.-P. Lange, *Angew. Chem. Int. Ed.* 54 (2015) 13186–13197.
- [59] B.C.E. Makhubela, J. Darkwa, *Johnson Matthey Technol.* 62 (2018) 4–31.
- [60] K.-R. Hwang, I.-H. Choi, H.-Y. Choi, J.-S. Han, K.-H. Lee, J.-S. Lee, *Fuel* 174 (2016) 107–113.
- [61] K. Mori, M. Dojo, H. Yamashita, *ACS Catal.* 3 (2013) 1114–1119.
- [62] S. Jones, A. Kolpin, S.C.E. Tsang, *Catal. Struct. React.* 1 (2015) 19–24.
- [63] X. Zhou, Y. Huang, W. Xing, C. Liu, J. Liao, T. Lu, *Chem. Commun.* (2008) 3540–3542.
- [64] H. Xiao, S.B. Lalvani, *J. Am. Oil Chem. Soc.* 84 (2007) 1177–1181.
- [65] T. Thananathanachon, T.B. Rauchfuss, *Angew. Chem. Int. Ed.* 49 (2010) 6616–6618.
- [66] L. Hu, L. Lin, S. Liu, *Ind. Eng. Chem. Res.* 53 (2014) 9969–9978.
- [67] J. Tuteja, H. Choudhary, S. Nishimura, K. Ebitani, *ChemSusChem* 7 (2014) 96–100.
- [68] L. Jicsinsky, R. Iványi, *Carbohydr. Polym.* 45 (2001) 139–145.
- [69] X. Tang, X. Zeng, Z. Li, L. Hu, Y. Sun, S. Liu, T. Lei, L. Lin, *Renew. Sust. Energy Rev.* 40 (2014) 608–620.
- [70] D. Kopetzki, M. Antonietti, *Green Chem.* 12 (2010) 656–660.
- [71] K. Fulajtárová, M. Hronec, T. Liptaj, N. Prónayová, T. Soták, *J. Taiwan Inst. Chem. E* 66 (2016) 137–142.
- [72] L. Liguori, T. Barth, *J. Anal. Appl. Pyrol.* 92 (2011) 477–484.
- [73] M. Oregui Bengoechea, A. Hertzberg, N. Miletić, P.L. Arias, T. Barth, *J. Anal. Appl. Pyrol.* 113 (2015) 713–722.
- [74] A. Toledano, L. Serrano, A. Pineda, A.A. Romero, R. Luque, J. Labidi, *Appl. Catal. B Environ.* 145 (2014) 43–55.
- [75] R. Nie, X. Peng, H. Zhang, X. Yu, X. Lu, D. Zhou, Q. Xia, *Catal. Sci. Technol.* 7 (2017) 627–634.
- [76] A.K. Singh, S. Jang, J.Y. Kim, S. Sharma, K.C. Basavaraju, M.-G. Kim, K.-R. Kim, J.S. Lee, H.H. Lee, D.-P. Kim, *ACS Catal.* 5 (2015) 6964–6972.
- [77] K. Tedsree, T. Li, S. Jones, C.W.A. Chan, K.M.K. Yu, P.A.J. Bagot, E.A. Marquis, G.D.W. Smith, S.C.E. Tsang, *Nat. Nanotechnol.* 6 (2011) 302–307.
- [78] J.C. Jansen, Z. Shan, L. Marchese, W. Zhou, Nvd. Pui, T. Maschmeyer, *Chem. Commun.* (2001) 713–714.
- [79] Z. Shan, P.W.G. Waller, B.G. Maingay, P.J. Angevine, J.C. Jansen, C.Y. Yeh, T. Maschmeyer, F.M. Dautzenberg, L. Marchese, H.O. Pastore, Zeolite Composite, Method for Making and Catalytic Application Thereof, US 7084087 B2 (2006).
- [80] Z. Shan, W. Zhou, J.C. Jansen, C.Y. Yeh, J.H. Koegler, T. Maschmeyer, A. Sayari, M. Jaronic (Eds.), *Studies in Surface Science and Catalysis*, Elsevier, 2002, pp. 635–640.
- [81] X.-Y. Quek, D. Liu, W.N.E. Cheo, H. Wang, Y. Chen, Y. Yang, *Appl. Catal. B Environ.* 95 (2010) 374–382.
- [82] C. Simons, U. Hanefeld, I.W.C.E. Arends, R.A. Sheldon, T. Maschmeyer, *Chem. Eur. J.* 10 (2004) 5829–5835.
- [83] S. Lima, M.M. Antunes, A. Fernandes, M. Pillinger, M.F. Ribeiro, A.A. Valente, *Molecules* 15 (2010) 3863–3877.
- [84] J.M. Campelo, F. Lafont, J.M. Marinas, *J. Chem. Soc. Faraday Trans.* 91 (1995) 1551–1555.
- [85] S. Chandra Shekar, J. Krishna Murthy, P. Kanta Rao, K.S. Rama Rao, *J. Mol. Catal. A Chem.* 191 (2003) 45–59.
- [86] S. Bhogswararao, D. Srinivas, *J. Catal.* 327 (2015) 65–77.
- [87] N.K. Kotsev, L.I. Ilieva, *Catal. Lett.* 18 (1993) 173–176.
- [88] N.W. Hurst, S.J. Gentry, A. Jones, B.D. McNicol, *Catal. Rev.* 24 (1982) 233–309.
- [89] N. Seshu Babu, N. Lingaiah, P.S. Sai Prasad, *Appl. Catal. B Environ.* 111–112 (2012) 309–316.
- [90] R. Moreno-Tost, J. Santamaría-González, P. Maireles-Torres, E. Rodríguez-Castellón, A. Jiménez-López, *J. Mater. Chem.* 12 (2002) 3331–3336.
- [91] S. Sithisa, W. An, D.E. Resasco, *J. Catal.* 284 (2011) 90–101.
- [92] J. Lee, Y.T. Kim, G.W. Huber, *Green Chem.* 16 (2014) 708–718.
- [93] L. Gucci, *Catal. Rev.* 23 (1981) 329–376.
- [94] F.J. Berry, X. Changhai, S. Jobson, *J. Chem. Soc. Faraday Trans* 86 (1990) 165–169.
- [95] T. Alammur, O. Shekhah, J. Wohlgemuth, A.-V. Mudring, *J. Mater. Chem.* 22 (2012) 18252–18260.
- [96] S. BR, J. XR, J. Theor. Comput. Sci. 3 (2016) 1–10.
- [97] Y. Xu, S. Qiu, J. Long, C. Wang, J. Chang, J. Tan, Q. Liu, L. Ma, T. Wang, Q. Zhang, *RSC Adv.* 5 (2015) 91190–91195.
- [98] J. Feroso, M.V. Gil, F. Rubiera, D. Chen, *ChemSusChem* 7 (2014) 3063–3077.
- [99] Z. Tan, X. Xu, Y. Liu, C. Zhang, Y. Zhai, P. Liu, Y. Li, R. Zhang, *Environ. Prog. Sustain.* 33 (2014) 751–755.
- [100] L.M. Esteves, M.H. Brijaldo, F.B. Passos, *J. Mol. Catal. A Chem.* 422 (2016) 275–288.
- [101] G.B. Kok, P.J. Scammells, *RSC Adv.* 2 (2012) 11318–11325.
- [102] I. Primožič, M. Bolant, A. Ramić, S. Tomić, *Molecules* 17 (2012) 786.
- [103] M. Anbazhagan, D.W. Boykin, C.E. Stephens, *Synthesis* 16 (2003) 2467–2469.
- [104] X. Hu, R.J.M. Westerhof, L. Wu, D. Dong, C.-Z. Li, *Green Chem.* 17 (2015) 219–224.
- [105] X. Hu, Y. Song, L. Wu, M. Gholizadeh, C.-Z. Li, *ACS Sustain. Chem. Eng.* 1 (2013) 1593–1599.
- [106] F. Yu, R. Zhong, H. Chong, M. Smet, W. Dehaen, B.F. Sels, *Green Chem.* 19 (2017) 153–163.
- [107] T. Katayama, T. Nitta, *J. Chem. Eng. Data* 21 (1976) 194–196.
- [108] M.S. Wainwright, T. Ahn, D.L. Trimm, N.W. Cant, *J. Chem. Eng. Data* 32 (1987) 22–24.
- [109] J.V.H. d'Angelo, A.Z. Francesconi, *J. Chem. Eng. Data* 46 (2001) 671–674.
- [110] D.D. Bank, *Thermophysical Data for Process Design*, DDBST GmbH, (2018) Accessed 31 January 2018 <http://www.ddbst.com/ddbst.html>.
- [111] P. Panagiotopoulou, N. Martin, D.G. Vlachos, *J. Mol. Catal. A Chem.* 392 (2014) 223–228.
- [112] L. Grazia, D. Bonincontro, A. Lolli, T. Tabanelli, C. Lucarelli, S. Albonetti, F. Cavani, *Green Chem.* 19 (2017) 4412–4422.
- [113] P. Yang, Q. Xia, X. Liu, Y. Wang, *Fuel* 187 (2017) 159–166.
- [114] X. Chang, A.F. Liu, B. Cai, J.Y. Luo, H. Pan, Y.B. Huang, *ChemSusChem* 9 (2016) 3330–3337.
- [115] B. Wang, C. Li, B. He, J. Qi, C. Liang, *J. Energy Chem.* 26 (2017) 799–807.
- [116] Z. Fu, Z. Wang, W. Lin, W. Song, S. Li, *Appl. Catal. A Gen.* 547 (2017) 248–255.
- [117] Z. Fu, Z. Wang, W. Lin, W. Song, *Energy Source Part A* 39 (2017) 1176–1181.
- [118] M. Li, L. Collado, F. Cárdenas-Lizana, M.A. Keane, *Catal. Lett.* 148 (2018) 90–96.
- [119] B. Seemala, C.M. Cai, R. Kumar, C.E. Wyman, P. Christopher, *ACS Sustain. Chem. Eng.* 6 (2018) 2152–2161.
- [120] N. Pino, S. Sithisa, Q. Tan, T. Souza, D. López, D.E. Resasco, *J. Catal.* 350 (2017) 30–40.
- [121] C.P. Jiménez-Gómez, J.A. Cecilia, R. Moreno-Tost, P. Maireles-Torres, *ChemSusChem* 10 (2017) 1448–1459.
- [122] X. Yang, X. Xiang, H. Chen, H. Zheng, Y.W. Li, Y. Zhu, *ChemCatChem* 9 (2017) 3023–3030.
- [123] C.P. Jiménez-Gómez, J.A. Cecilia, R. Moreno-Tost, P. Maireles-Torres, *ChemCatChem* 9 (2017) 2881–2889.
- [124] S. Srivastava, G.C. Jadeja, J. Parikh, *J. Mol. Catal. A Chem.* 426 (2017) 244–256.
- [125] C.P. Jiménez-Gómez, J.A. Cecilia, I. Márquez-Rodríguez, R. Moreno-Tost, J. Santamaría-González, J. Mérida-Robles, P. Maireles-Torres, *Catal. Today* 279 (2017) 327–338.
- [126] W. Gong, C. Chen, H. Zhang, G. Wang, H. Zhao, *ChemistrySelect* 2 (2017) 9984–9991.
- [127] G.S. Hutchings, W. Luc, Q. Lu, Y. Zhou, D.G. Vlachos, F. Jiao, *Ind. Eng. Chem. Res.* 56 (2017) 3866–3872.
- [128] E.I. Grizorashvili, N.S. Zolotarev, A.A. Buimov, V.I. Sirotenko, N.V. Shavolina,

- I.M. Lisnyanskii, *Pharm. Chem. J. USSR* 6 (1969) 357.
- [129] L.W. Burnett, I.B. Johns, R.F. Holdren, R.M. Hixon, *Ind. Eng. Chem.* 40 (1948) 502–505.
- [130] O.F. Aldosari, S. Iqbal, P.J. Miedziak, G.L. Brett, D.R. Jones, X. Liu, J.K. Edwards, D.J. Morgan, D.K. Knight, G.J. Hutchings, *Catal. Sci. Technol.* 6 (2016) 234–242.
- [131] M.G. Dohade, P.L. Dhepe, *Clean Technol. Environ.* (2017) 1–11.
- [132] C. Wang, J. Luo, V. Liao, J.D. Lee, T.M. Onn, C.B. Murray, R.J. Gorte, *Catal. Today* 302 (2018) 73–79.
- [133] F. Dong, Y. Zhu, H. Zhao, Z. Tang, *Catal. Sci. Technol.* 7 (2017) 1880–1891.
- [134] J. Cui, J. Tan, X. Cui, Y. Zhu, T. Deng, G. Ding, Y. Li, *ChemSusChem* 9 (2016) 1259–1262.
- [135] F. Dong, G. Ding, H. Zheng, X. Xiang, L. Chen, Y. Zhu, Y. Li, *Catal. Sci. Technol.* 6 (2016) 767–779.
- [136] F. Dong, Y. Zhu, H. Zheng, Y. Zhu, X. Li, Y. Li, *J. Mol. Catal. A Chem.* 398 (2015) 140–148.
- [137] T. Wang, K. Li, Q. Liu, Q. Zhang, S. Qiu, J. Long, L. Chen, L. Ma, Q. Zhang, *Appl. Energy* 136 (2014) 775–780.
- [138] J. Lessard, J.-F. Morin, J.-F. Wehrung, D. Magnin, E. Chornet, *Top. Catal.* 53 (2010) 1231–1234.
- [139] H.-Y. Zheng, Y.-L. Zhu, L. Huang, Z.-Y. Zeng, H.-J. Wan, Y.-W. Li, *Catal. Commun.* 9 (2008) 342–348.
- [140] H.-Y. Zheng, Y.-L. Zhu, Z.-Q. Bai, L. Huang, H.-W. Xiang, Y.-W. Li, *Green Chem.* 8 (2006) 107–109.
- [141] K. Opwus, T. Mayer-Gall, J.S. Gutmann, Recovery of noble metals from industrial process waters by the use of functional textiles, CEST 2017- 15th International Conference on Environmental Sciences and Technology, Rhodes, Greece, 2017.
- [142] M.J. Gilkey, P. Panagiotopoulou, A.V. Mironenko, G.R. Jenness, D.G. Vlachos, B. Xu, *ACS Catal.* 5 (2015) 3988–3994.
- [143] T.T. Pham, S.P. Crossley, T. Sooknoi, L.L. Lobban, D.E. Resasco, R.G. Mallinson, *Appl. Catal. A Gen.* 379 (2010) 135–140.
- [144] M.G. Dohade, P.L. Dhepe, *Green Chem.* 19 (2017) 1144–1154.
- [145] S. Sitthisa, T. Pham, T. Prasomsri, T. Sooknoi, R.G. Mallinson, D.E. Resasco, *J. Catal.* 280 (2011) 17–27.
- [146] M. Mavrikakis, M.A. Barteau, *J. Mol. Catal. A Chem.* 131 (1998) 135–147.
- [147] J.L. Davis, M.A. Barteau, *J. Am. Chem. Soc.* 111 (1989) 1782–1792.
- [148] Y. Chen, Z. Guo, T. Chen, Y. Yang, *J. Catal.* 275 (2010) 11–24.
- [149] Y. Shim, Y. Itoh, K. Wakita, N. Mamedov, *Appl. Surf. Sci.* 421 (2017) 788–793.

**Update**

**Applied Catalysis B: Environmental**

Volume 243, Issue , April 2019, Page 801

DOI: <https://doi.org/10.1016/j.apcatb.2018.08.032>



## Corrigendum

# Corrigendum to “One-pot hydrogen production and cascade reaction of furfural to bioproducts over bimetallic Pd-Ni TUD-1 type mesoporous catalysts” [Appl. Catal. B: Environ. 237 (2018) 521–537]

Margarida M. Antunes<sup>a</sup>, Sérgio Lima<sup>b</sup>, Auguste Fernandes<sup>c</sup>, Maria F. Ribeiro<sup>c</sup>, David Chadwick<sup>b</sup>, Klaus Hellgardt<sup>c</sup>, Martyn Pillinger<sup>a</sup>, Anabela A. Valente<sup>a,\*</sup>

<sup>a</sup> Department of Chemistry, CICECO-Aveiro Institute of Materials, University of Aveiro, Campus Universitário de Santiago, 3810-193 Aveiro, Portugal

<sup>b</sup> Department of Chemical Engineering, Imperial College London, South Kensington Campus, London SW7 2AZ, UK

<sup>c</sup> Institute for Biotechnology and Bioengineering, Centre for Biological and Chemical Engineering, Instituto Superior Técnico, Av. Rovisco Pais, 1049-001 Lisbon, Portugal



The authors regret that the names of the chemical compounds 2-(ethoxymethyl)furan, 2-(butoxymethyl)furan and 2-(alkoxymethyl)furan were published with systematic error. The names “2-ethoxyfuran”, “2-butoxyfuran” and “2-alkoxyfuran” should always read “2-(ethoxymethyl)furan”, “2-(butoxymethyl)furan” and “2-(alkoxymethyl)furan”, respectively. The name and chemical structure of 2-(alkoxymethyl)furan were published with error in Schemes 1 and 2; the chemical structure is reproduced correctly bellow. These corrections do not change or compromise the catalytic results and discussion of the original article.

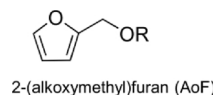


Table 3 includes data for bimetallic catalysts only (please ignore “mono-” in its title).

The authors would like to apologise for any inconvenience caused.

DOI of original article: <https://doi.org/10.1016/j.apcatb.2018.06.004>

\* Corresponding author.

E-mail address: [atav@ua.pt](mailto:atav@ua.pt) (A.A. Valente).

<https://doi.org/10.1016/j.apcatb.2018.08.032>

Available online 27 September 2018

0926-3373/ © 2018 Published by Elsevier B.V.